Non-targeted Stressful Effects in Normal Human Fibroblast Cultures Exposed to Low Fluences of High Charge, High-Energy (HZE) Particles: Kinetics of Biologic Responses and Significance of Secondary Radiations.

Géraldine Gonon, Jean-Emmanuel Groetz, Sonia M de Toledo, Roger W Howell, Michel Fromm, Edouard I Azzam

Non-Targeted Stressful Effects in Normal Human Fibroblast Cultures Exposed to Low Fluences of High Charge, High Energy (HZE) Particles: Kinetics of Biologic Responses and Significance of Secondary Radiations

Géraldine Gonon[a,b], Jean-Emmanuel Groetz[b], Sonia M. de Toledo[a], Roger W. Howell[a], Michel Fromm[b,1] and Edouard I. Azzam[a,2]

[a]Department of Radiology, UMDNJ - New Jersey Medical School Cancer Center, Newark, NJ 07103, USA

[b]Laboratoire de Chimie Physique et Rayonnements - Alain Chambaudet (LCPR-AC), LRC CEA, UMR CNRS 6249 Chrono-Environnement, Université de Franche-Comté, Besançon, France

Running head: HZE-PARTICLE-INDUCED BYSTANDER EFFECTS

Key words: bystander effects, space exploration, radiation protection, hadron therapy, HZE ion fragmentation, secondary radiation

Manuscript Category: Regular Paper

Number of Pages: 44
Number of Figures: 6
Number Tables: 2
Supplementary Figures: 1; Supplementary Tables: 4

[1,2]Addresses for correspondence:

Edouard Azzam
Department of Radiology
UMDNJ – New Jersey Medical School
Cancer Center
205 South Orange Avenue
Cancer Center Bldg. – Room F1212
Newark, NJ 07103
Phone: 973-972-5323
Fax: 973-972-1865
E-mail: azzamei@umdnj.edu

Michel Fromm
Laboratoire de Chimie Physique et Rayonnements - Alain Chambaudet (LCPR-AC), LRC CEA, UMR CNRS 6249 Chrono-Environnement
Université de Franche-Comté,
16 route de Gray
F-25030 Besançon Cedex, France
Phone: (0) 33 3 81 66 65 60
Fax: (0) 33 3 81 66 65 22
E-mail: michel.fromm@univ-fcomte.fr

ABSTRACT

The induction of non-targeted stressful effects in cell populations exposed to low fluences of high charge (Z) and high energy (E) particles is relevant to estimates of the health risks of space radiation. We investigated the upregulation of stress markers in confluent normal human fibroblast cultures exposed to 1000 MeV/u iron ions (linear energy transfer (LET) ~151 keV/μm) or 600 MeV/u silicon ions (LET ~50 keV/μm) at mean absorbed doses as low as 0.2 cGy, wherein 1-3 % of the cells were targeted through the nucleus by a primary particle. Within 24 h post-irradiation, significant increases in the levels of phospho-TP53 (serine 15), $p21^{Waf1}$ (CDKN1A), HDM2, phospho-ERK1/2, protein carbonylation and lipid peroxidation were detected, which suggested participation in the stress response of cells not targeted by primary particles. This was supported by *in situ* studies that indicated greater increases in 53BP1 foci formation, a marker of DNA damage, than expected from the number of primary particle traversals. The effect was expressed as early as 15 min after exposure, peaked at 1 h, and decreased by 24 h. A similar tendency occurred after exposure of the cell cultures to 0.2 cGy of 3.7 MeV α particles (LET ~109 keV/μm) that targets ~1.6 % of nuclei, but not after 0.2 cGy from 290 MeV/u carbon ions (LET ~13 keV/μm) by which, on average, ~13 % of the nuclei were hit, which highlights the importance of radiation quality in the induced effect. Simulations with the FLUKA multi-particle transport code revealed that fragmentation products, other than electrons, in cell cultures exposed to HZE particles comprise <1 % of the absorbed dose. Further, the radial spread of dose due to secondary heavy ion fragments is confined to approximately 10-20 μm. Thus, the latter are unlikely to significantly contribute to stressful effects in cells not targeted by primary HZE particles.

INTRODUCTION

The ionizing radiation-induced bystander effect has been broadly defined as the induction of biological changes in in cells not directly targeted by radiation (*1*). Stressful bystander effects have been extensively observed in cell populations where only a small fraction of the cells is targeted by high linear energy transfer (LET) α particles. Induction of genetic alterations, including sister chromatid exchanges (*2*), mutations (*3, 4*), chromosomal aberrations (*5*) and micronuclei (*6*), changes in gene expression (*7, 8*), lethality (*9*) and neoplastic transformation (*10, 11*) have been observed in bystander cells of various lineages after exposure of other cells to α particles. On the other hand, the characterization of bystander effects in cell cultures exposed to very low fluences of high charge (Z) and high energy (E) (HZE) particles, another type of high LET radiation, are only emerging, and conflicting data have been reported. In initial experiments with microbeam, stressful effects were shown to be transmitted from HZE-particle-irradiated cells to contiguous cells that were not targeted by the primary particle (*12-14*). In subsequent experiments whereby HZE-particle-irradiated cells were co-cultured with bystander cells in a manner that they only shared growth medium, stressful responses were also induced in the bystander cells and were similar in nature to those generated in the targeted cells (*15-17*). Furthermore, oxidative stress and DNA damage persisted in distant progeny of bystander cells that had been in contiguous co-culture with HZE-particle-irradiated cells (*18, 19*). However, other experiments involving the transfer of growth medium from irradiated cultures to recipient bystander cells present in a separate dish (*9, 20*), or the targeting of an exact number of cells in a population with energetic heavy ions from a microbeam (*21*) did not detect an effect with a variety of endpoints and

cell types. Several factors may underlie the absence of observable effects in these cases, including timing of endpoint measurement, dilution of the inducing factor and the metabolic state/redox environment of the recipient cells.

Providing clear evidence for HZE-particle-induced bystander effects is pertinent to space exploration during which astronauts are likely to be exposed to low fluences of energetic particles (*22*). To gain greater knowledge of HZE-particle-induced bystander effects, we investigated the expression of stress markers in density-inhibited normal human diploid fibroblast cultures exposed to low fluences of iron, silicon or carbon ions, and compared the results with those obtained in cultures exposed to low fluences of α particles. The data showed clear evidence for modulation of $p53/p21^{Waf1}$ and ERK1/2 signaling in cultures exposed to doses as low as 0.2 cGy wherein only 1-3 % of nuclei are traversed by a primary particle track. An increase in protein carbonylation and lipid peroxidation was also detected at 24 h after exposure, suggesting that perturbations in oxidative metabolism contribute to the greater than expected stressful effects, based on microdosimetric considerations of the fraction of cells traversed by a primary particle. *In situ* immune-detection studies of 53BP1 foci formation, a marker that has been associated with DNA double strand breaks (*23*), together with the use of culture dishes where a solid-state nuclear track detector was fused to the glass bottom on which the cells grow, supported the involvement of cells not targeted by primary HZE particles in the response of cell cultures to radiation.

The microscopic structure of the primary HZE-particle-track is characterized by a high frequency of interactions with the target, which result in highly localized energy depositions (*24, 25*). Secondary radiations arise from interactions with atomic electrons

in target atoms and from fragmentation of the incident HZE particle and target nuclei. These secondaries are produced along the primary particle track and include energetic electrons (δ rays), photons, protons, neutrons, α particles and other heavier ions with different LET values. In contrast to δ rays with a maximum range of ~0.1 μm that are produced in biological matter when traversed by the 2-10 MeV high-LET α particles that are emitted during α decay of radionuclides (*26*), the range of δ rays produced following HZE particle-traversals can extend up to several cell diameters (*27, 28*), thereby potentially irradiating and contributing to biochemical changes in cells that are near those targeted by the primary particle track. In particular, protective mechanisms induced by low LET secondary radiations may mitigate stressful effects propagated from cells traversed by the primary particle (*29*). Alternatively, cells that were thought to be bystanders may be significantly irradiated by secondaries. To investigate whether secondary particles are a factor in apparent HZE-particle-induced bystander effects, the tracks of the secondaries were simulated with the multi-particle transport code FLUKA and absorbed doses received by the monolayer of cells adjacent to the targeted cells were assessed (*30-32*).

MATERIALS AND METHODS

Cell culture

AG1522 normal human diploid skin fibroblasts were obtained from the Genetic Cell Repository at the Coriell Institute for Medical Research. Cells at passage 10-12 were grown in Eagles' Minimum Essential Medium (MEM) (CellGro) containing 12.5 % (vol/vol) heat inactivated (30 min at 56 ºC) fetal bovine serum (FBS) (Sigma), supplemented with 4 m*M* L-alanyl-L-glutamine (CellGro), 100 U/mL penicillin and

100 µg/mL streptomycin (CellGro). They were maintained in 37 ºC humidified incubators in an atmosphere of 5 % CO_2 (vol/vol) in air. For experiments, cells were seeded at numbers that allowed them to reach the density-inhibited state within 5 days. They were then fed twice on alternate days, and experiments were initiated 48 h after the last feeding. Under these conditions, 95-98 % of cells were in G_0/G_1 phase of the cell cycle. The synchronization of cells in G_0/G_1 phase, by density-inhibition of growth, eliminates complications in interpretation of results that arise from changes in responses to ionizing radiation at different phases of the cell cycle (*33*).

For HZE-particle-irradiation, the cells were either grown in 25 cm^2 polystyrene flasks (Greiner) for Western blot analyses or in glass-bottomed flaskettes (Nalge Nunc International) for *in situ* detection of 53BP1 foci. Cells destined for α-particle-irradiation were seeded in stainless steel dishes with a circular 36-mm-diameter growing surface that consists of 1.5 µm-thick replaceable polyethylene terephthalate (PET). To facilitate cell attachment, the PET surface was precoated with FNC solution comprising fibronectin and collagen (AthenaES™), overlaid with 2 mL of MEM and incubated at 37 ºC. After 30 min, the medium was aspirated and the cells were seeded.

Culture dishes with nuclear track detector bottom and etching

To identify cells irradiated by a primary particle, a 100 µm-thick polyallyl diglycol carbonate (PADC) plastic polymer (Tastrak™ from Track Analysis Systems Ltd., commonly known as Columbia Resin #39 or CR-39™ plastic) was grafted to the glass bottom of tissue culture dishes (Ibidi®) as shown in Supplementary Figure 1, Panel B. Upon cell fixation, the PADC was etched in 10 mol/L KOH at 37 ºC for 3.5 h and the pits were visualized by light microscopy. *In situ* analyses of 53BP1 foci were

performed following etching. Images were obtained by switching from fluorescent to optical imaging and changing the focal plane. Monitoring of confluent cultures during a 3 h period by confocal microscopy using a fixed high magnification field did not reveal any movement of the cells following exposure to mean absorbed doses of 0.1-0.3 cGy of α particles (*34*).

Irradiation and dosimetry

Irradiation with 1000 MeV/u $^{56}Fe^{26+}$, 600 MeV/u $^{28}Si^{14+}$ or 290 MeV/u $^{12}C^{6+}$ with LET in liquid water of ~151 keV/µm, ~50 keV/µm and ~13 keV/µm, respectively, were performed at the NASA Space Radiation Laboratory (NSRL) at Brookhaven National Laboratory (Upton, NY) during 2008-2011. The monolayers were positioned perpendicularly to the beam in the plateau region of the Bragg curve, but were not stacked (profiles of the ions' Bragg curves can be accessed at http://www.bnl.gov/medical/NASA/CAD/Bragg_Curves.asp). The flasks were filled to capacity, 3 h prior to irradiation, with pH and temperature-equilibrated growth medium containing 20 % (vol/vol) conditioned medium that was harvested from confluent AG1522 cell cultures grown for 48 h. This ensured that, during the irradiation, deviation from 37 °C was attenuated and the cells were immersed in medium, which alleviates changes in osmolarity and partial oxygen tension. The latter parameters greatly affect the cellular responses to radiation (*35, 36*). The foam sample-holder produces minimal scatter or fragmentation of the incoming heavy ion beam (www.bnl.gov/medical/NASA/CAD/Sample_Holder_Layout.asp). Exposures to 0.2 or 1 cGy occurred at dose rates of 0.2 and 1 cGy/min, respectively. The dose of 0.2 cGy was delivered in 3 or 4 spills at a minimum. Uniformity of the beam across the irradiated flasks was between 1 % and 5 %.

The dose just out of the beam (i.e. the beam-related background) is proportional to the beam dose and is on the order of 0.01 % of the dose in the beam. The background radiation due to activation depended on the preceding irradiation; in case our experiment was preceded by a 1 h exposure to the maximum rate of protons delivered at the NSRL, the γ ray dose that cells would receive would be at the rate of ~10^{-5} cGy/min. Sham-irradiated cell cultures served as control and were handled similarly as the test cultures.

Alpha-particle-irradiations were conducted with a 7.4 MBq ^{241}Am collimated source housed in a helium-filled Plexiglas box located in a chamber at 37 ºC with an atmosphere of 5 % CO_2 (vol/vol) in air. To optimize uniformity of the beam, the source was mounted on a rotating platform (88 rpm) and the exit window was equipped with a beam delimiter. The uniformity was confirmed by etching PADC plastic exposed to the beam for 4 seconds. Cells were irradiated at a mean absorbed dose rate of 2 cGy/min, and irradiation of samples occurred from below through the PET growing surface. At the latter surface, α particles had a measured mean energy of 3.7 MeV (0.92 MeV/u) with Full Width at Half Maximum (FWHM) of 0.5 MeV. The LET corresponding to a mean energy of 3.7 MeV is ~109 keV/µm in liquid water. The irradiator box was fitted with a photographic shutter to allow accurate delivery of the desired mean absorbed dose (*37*).

The fluence ϕ of HZE particles was determined by PMT/Scintillator-based dosimetry; it was then used to calculate the mean dose to the cell population according to the relation ϕ (particles/cm^2) = [D (cGy) ρ (g/cm^3)] / [1.602×10^{-7} LET (keV/µm)], where D is the mean dose and ρ is the density. In case of α-particle-irradiation, the fluence ϕ for a fixed dose was estimated based on previous measurements (*37*). The average number of nuclear and cellular particle traversals was calculated by multiplying

the fluence with the average cross-section of an AG1522 cell nucleus (i.e. 140 μm^2 (*7*)) or with the average cross-sectional area of an AG1522 whole cell (i.e. 800 μm^2 (*34*) measured in confluent cultures grown under similar conditions as in this study). The calculations of fluence were confirmed after etching of PADC. Estimates of the fractions of whole cells or nuclei traversed by a primary particle were calculated assuming Poisson statistics and are given in Table 1. These values were determined according to the method of Charlton and Sephton (*38*), where the probability P that a given target area is traversed by N particles is given by $P(N) = e^{-x} x^N/N!$ with x being the product of the fluence and the target cross-sectional area (nucleus or whole cell).

Secondary radiations

In this work, for studies of *in situ* detection of 53BP1 foci, the HZE particles traversed first the soda-lime glass bottom of the flaskettes before reaching the cells and growth medium. Some of the HZE interactions with these target materials may result in fragmentation of the incident (*i.e.* primary) particle and/or of the target material. Fragmentation of the incident HZE particle may produce lower-atomic number (Z) fragments. The primary-particle fragments have a high probability of proceeding with the same velocity as the primary particle, whereas target fragments generally have lower velocity and can be scattered with respect to the incident-ion-trajectory (*25*). Photons and secondary electrons (δ rays), generated as a result of these interactions, can travel, depending on their energy, significant distances away from the primary particle track (*39*).

To determine whether secondary particles impart a significant absorbed dose to either directly targeted cells, or cells in the vicinity, when a mean absorbed dose of

0.2 cGy is delivered with either 1000 MeV/u ^{56}Fe ions, 600 MeV/u ^{28}Si ions or 290 MeV/u ^{12}C ions, calculations were undertaken, using FLUKA code version 2011.2.15 (*31, 32, 40*) with the default configuration 'HADROTHErapy'. FLUKA is a multi-purpose Monte Carlo particle transport code that considers all particle interactions including electromagnetic interactions, nuclear interactions of the primary or incident particles and the generated secondary particles, energy loss fluctuations and Coulomb scattering.

Several parameters were considered in our simulations with FLUKA. They included transport threshold for particles, delta ray production threshold, and restricted ionization fluctuations. The RQMD model was used, since its interface was developed for the processing of ion-ion interactions from 0.1 GeV/u to 5 GeV/u. The event generators RQMD and DPMJET were linked to ensure ion-ion interactions above 125 MeV/u. The FLUKA evaporation/fission/fragmentation module performed the fragmentation of the primary heavy ions and the de-excitation of the excited fragments. Simulations were undertaken with the transport cut-offs for heavy ions (primary and fragments), photons, protons and α particles set at 1 keV. The transport cut-off for electrons was set at 1 keV when the production threshold for δ rays was 10, 100, and 1000 keV; it was set at 150 eV when the production threshold for δ rays was 1 keV. Production thresholds for δ rays were set at equal value in the cover slip, cell monolayer and medium to ensure that the electronic equilibrium is established (i.e. that the flux of secondary electrons leaving a surface is independent of the surface thickness). This would be a sensitive parameter for a very thin surface like the cell monolayer. Upon reaching the cut-off energy, the particles

were assumed to deposit this cut-off energy locally and their tracks were no longer followed.

The contribution of neutrons to the absorbed was calculated but is not shown due to inconsistent results, especially in the cell monolayer. Since the HADROTHErapy option was used, neutrons with energy below 20 MeV cannot be followed with dedicated multi-group library for neutrons with that energy. Benchmarking the FLUKA code with the MCNP code could generate more consistent results for the neutron dose.

Using FLUKA, the radial dose distribution to the AG1522 cell monolayer around the track of a narrow beam of 1000 MeV/u ^{56}Fe ions was calculated for both the primary particle and its secondaries (HADRONTHErapy configuration with delta rays' production thresholds set at 1, 10, 100, and 1000 keV). Every run was performed with 10^5 ions, and the absorbed doses to concentric annuli (thickness 1 μm, depth 1 μm) extending to a radius of 100 μm were calculated. The radial distance of 100 μm covers the diameter of an AG1522 cell and extends to adjacent cells.

To recreate experimental conditions, the geometry and the constitutive materials of the flaskettes were introduced into the FLUKA input file. The beam spot at the NSRL has a uniform center of 20 cm x 20 cm. Within this area, the flaskette containing the cell monolayer was recreated (Supplementary Figure 1, Panel A). The cell monolayer was characterized by an area of 10 cm^2 and thickness of 1 μm (i.e. height up to the center of the nucleus) (*41*)[1]. The 1 mm-thick soda-lime glass was 19.152 cm^2 in area. The corresponding volumes were 0.001 and 1.92 cm^3, respectively, and the volume of the culture medium was 18.8 cm^3. The elemental mole percentages of the soda-lime glass

[1] The thickness of ~1 μm of an AG1522 cell (*41*) was estimated from studies in fixed/dehydrated cells grown on Mylar. The actual dimension of a live AG1522 cell grown on glass may be different.

(ρ ~2.33 g/cm^3) were O (60 %), Si (25 %), Na (10 %), Ca (3 %), Mg (1 %) and Al (1 %). The 1 mm-thick polystyrene (C_8H_8) walls of the flaskettes have a density of 1.06 g/cm^3. The cell monolayer was assumed to be composed of human skin equivalent (W&W type 3 (*42*)) with elemental mass composition of H (10.1 %), C (15.8 %), N (3.7 %), O (69.5 %), S (0.2 %), Cl (0.3 %), Na (0.2 %) and K (0.1 %) and with a density of 1.09 ± 0.05 g/cm^3. For simplicity, the growth medium was considered to be water with a thickness of 1.87 cm (flaskette is filled to capacity with culture medium). The flaskette, thus modeled, was oriented vertically and its growth surface was orthogonal to the incident beam. The doses calculated by FLUKA were provided as GeV/g cm^3/primary ion. Radiation absorbed doses in cGy (Table 2 and Supplementary Tables 2-4) were obtained from the FLUKA output by correcting the values for target volume and the fluence. The fluence of 8323 ^{56}Fe-ions/cm^2 was experimentally determined at BNL by scintillator-based dosimetry, which relies on counting the tracks in the beam. When a certain preset number of tracks with high LET characteristic was reached, the beam was cut-off. This approach was also used in the FLUKA simulations for determining the mean absorbed dose to the various targets from the primary and secondary radiations.

Western blot analyses

Following irradiation, the cells were harvested by trypsinization, pelleted, rinsed in PBS, repelleted, and lysed in chilled radio-immune precipitation assay (RIPA) buffer [50 m*M* Tris-CI (pH 7.5), 150 m*M* NaCI, 50 m*M* NaF, 5 m*M* EDTA, 1 % (vol/vol) NP40, 0.5 % (wt/vol) sodium deoxycholate, 0.1 % SDS] supplemented with sodium orthovanadate (1 m*M*), and protease (1:1000, vol/vol) and phosphatase (1:1000, vol/vol)

inhibitor cocktails (Sigma). The extracted proteins were fractionated by SDS-PAGE and immunoblotted.

Protein levels: Stress responsive proteins were quantified with antibodies against $p21^{Waf1}$ (05-345, Millipore), p-TP53ser15 (9284, Cell Signaling), p-ERK1/2 (9101, Cell Signaling) and HDM2 (M4308, Sigma).

Protein oxidation: When proteins are oxidized by reactive oxygen species (ROS), some amino acids are modified generating carbonyl groups. These carbonyl groups, specifically of aldehydes or ketones, can react with 2,4-dinitrophenyl hydrazine (DNPH), which may be recognized by anti-2,4 dinitrophenol (DNP) antibodies on immunoblots (*43*). For experiments, the OxyBlot Protein Oxidation Detection Kit (Millipore) was used. Protein samples were denaturated with 6 % (wt/vol) SDS and derivatized with DNPH. Negative controls were derivatized with a Derivatization-Control solution. After 15 min incubation at room temperature, neutralization solution (2 M Tris/30 % glycerol; vol/vol) was added and samples were immunoblotted. The DNPH-bound proteins were detected with rabbit anti-2,4-dinitrophenyl IgG (Millipore).

Accumulation of 4-hydroxynonenal adducts: Hydroxyalkenals, such as 4-hydroxynonenal (4-HNE), are among the major products of lipid peroxidation (*44*). Proteins with 4-HNE adducts were identified with goat anti-4-HNE antibody (Millipore).

After incubation of the nitrocellulose membranes with a specific secondary antibody conjugated with horseradish peroxidase, protein bands were detected by enhanced chemiluminescence system from GE Healthcare (Amersham). Luminescence was determined by exposure to X ray film, and densitometry analysis was performed with

an EPSON scanner and National Institutes of Health Image J software (NIH Research Services Branch).

Staining of the nitrocellulose membranes with Ponceau S Red (Sigma) was used to verify equal loading of samples (loading control) (*45*). Experiments were repeated 2 to 7 times, with separate experiments performed to evaluate changes in protein levels, protein oxidation and accumulation of 4-hydroxynonenal adducts. Representative data of immunoblots are shown in Results. Fold changes in the levels of stress responsive proteins in individual experiments together with mean ± standard error (SE) are reported in Supplementary Table 1. These changes include the responses of cells targeted by primary ions and those that are not. Treated samples were compared with the control of the respective time point.

In situ immune-detection of 53BP1

53BP1 is a marker of DNA double-strand breaks (DSB) (*46*). At different times after irradiation, confluent cells were rinsed twice in PBS, fixed with freshly prepared 3.2 % (vol/vol) paraformaldehyde in PBS for 10 min, and rinsed 5 times with PBS. Subsequently, the cells were permeabilized with Triton-X buffer (0.25 % Triton-X in water / 0.1 % saponin in Tris-buffered saline (TBS) [25 m*M* Tris, pH 7.5, 150 m*M* NaCl, 2 m*M* KCl in water] for 10 min. The fixed and permeabilized cell monolayers were then blocked for 1 h in blocking buffer [2 % (vol/vol) normal goat serum, 2 % (vol/vol) BSA, 0.1 % Triton X-100 (in TBS)] and reacted with rabbit anti-53BP1 antibody (A300-272A, Bethyl) diluted 1:500 (vol/vol) in blocking buffer and incubated for 2 h at room temperature. After incubation with Alexa Fluor 594 goat anti-rabbit secondary antibody (Invitrogen), the cells were washed 3 times (5 min/wash) in buffer consisting of 0.2 %

normal goat serum, 0.2 % BSA, 0.1 % Triton X-100 in TBS. SlowFade® Gold antifade reagent with DAPI (Invitrogen) was used in mounting the samples.

Cells with at least one 53BP1 focus were scored using a UV microscope (Leica DM IL). All the images within the same data set were captured with a ProgRes® camera (Jenoptik) with the same optics and exposure time and were saved for subsequent evaluation. As such, bleaching of the signal was avoided. Identical criteria were followed in defining foci characteristics. Nuclei with atypical size or morphology, and those with very high foci counts (presumably due to replication stress), were not scored (*47*). The data described in Results represent the excess percent increase of cells with 53BP1 foci in irradiated populations relative to respective control. They were calculated as follows:

$\Delta F = 100\ (F_{irradiated} - F_{control})$ where F is the ratio of the number of cells with 53BP1 foci over the total number of cells counted.

The results of three independent experiments for energetic iron and silicon ions and α particles are reported in Results. For each experiment, 2 irradiated and 2 control dishes were analyzed. For each dish, more than 3000 cells were scored by eye in 40 different fields. Poisson statistics was used to calculate the standard error associated with the percentage of cells with foci over the total number of cells scored. The Pearson's χ^2 test was used to compare treatment groups versus respective controls. A value of $p \leq 0.05$ between groups was considered significant.

A significant number of cells in control samples harbored foci, which fluctuated between experiments and assay times. When the control samples of all experiments were pooled, the mean ± SD of the fraction of cells harboring at least one 53BP1 focus was 0.26 ± 0.12 with a range of 0.05 to 0.50. The mean ± SD of spontaneous 53BP1 foci per

cell nucleus was 0.35 ± 0.12 with a range of 0.06 to 0.68 foci/cell. The mean ± SD of spontaneous 53BP1 foci per cell nucleus in foci-positive cells was 1.29 ± 0.11 foci/cell with a range from 1.04 to 1.35 foci/cell. These results are consistent with those of Ugenskiene et al. who estimated the background level of 53BP1 foci in AG1522 cells to be 1.1 foci/cell (*48*). A high background level of nuclear foci indicative of DNA damage was also observed in various cell strains, with inter and intra-individual differences being detected (*47*).

RESULTS

Significant biological changes are rapidly induced in normal human cell cultures exposed to low fluences of HZE particles

We investigated stress responses in normal human cell populations exposed to HZE particles under conditions where only a very small fraction of cells is traversed through the nucleus by a primary particle track. To this end, confluent AG1522 cell cultures were exposed to mean absorbed doses of 0.2 or 1 cGy of energetic iron or silicon ions. They were also exposed, in parallel, to α particles that have been shown to induce significant bystander effects (*2, 4, 6, 7*). We examined the phosphorylation of serine 15 in TP53 (p-TP53ser15), a marker of DNA damage (*49*), and of the stress-responsive extracellular signal-related kinases, ERK1 and ERK2 (p-ERK1/2) (*50*), at different times after irradiation. The observed changes were compared to those in respective controls.

At 15 min after exposure to mean absorbed doses of 0.2 or 1 cGy from 1000 MeV/u ^{56}Fe ions (LET ~151 keV/μm) or 600 MeV/u ^{28}Si (LET ~50 keV/μm), an increase in p-TP53ser15 and p-ERK1/2 levels was consistently observed (Figure 1, Panel A). Fold-increases of 1.7 ± 0.4 (n=3) and 2.3 ± 0.5 (n=3) in p-TP53ser15 levels,

and of 1.4 ± 0.1 (n=3) and 1.4 ± 0.1 (n=3) in p-ERK1/2 levels, were detected in cell cultures exposed to 0.2 cGy of ^{56}Fe or ^{28}Si ions, respectively (representative data shown in Figure 1, Panel A). At a mean absorbed dose of 0.2 cGy, only ~1.2 and 3.5 % of nuclei are traversed by either ion, respectively. Similarly, at 1 cGy, wherein ~6 % of nuclei are traversed by an iron ion and 17.5 % by a silicon ion, respective fold-increases of 3.2 ± 1 (n=6) and 2.9 ± 0.5 (n=4) in p-TP53ser15 levels, and of 2.7 ± 0.3 (n=5) and 2.4 ± 0.3 (n=4) in p-ERK1/2 levels, were observed (representative data shown in Figure 1, Panel A). Therefore, these data indicate that p-ERK1/2 and p-TP53ser15 are sensitive markers that are rapidly modulated after exposure of normal human cell cultures to very low mean absorbed doses of high-LET HZE radiations. The levels of p-TP53ser15 and p-ERK1/2 were similarly increased at 15 min after exposure of confluent AG1522 cell cultures to 0.2 cGy (1.5 ± 0.0 (n=4) and 1.2 ± 0.1 (n=3), respectively) or 1 cGy (2.1 ± 0.3 (n=7), and 2.2 ± 0.2 (n=6), respectively) of 3.7 MeV α particles (LET ~109 keV/μm) (representative data shown in Figure 1, Panel A). The increase in p-TP53ser15 level, correlated with increases in the levels of HDM2 and p21^{Waf1} at 1 h (Figure 1, Panel B) and 3 h (Figure 1, Panel C) after irradiation, suggesting activation of TP53, a central protein involved in maintenance of genomic integrity. Similar increases in TP53 signaling were also observed at 6 and 24 h after irradiation (Figure 1, Panel D). For all treatments, the results of individual experiments are described in supplementary Table 1.

Likewise, 3.3 ± 1.4 (n=3) and 6.5 ± 1.8 (n=3)-fold increases in overall protein carbonylation were detected in extracts of cell cultures harvested 24 h after exposure to 0.2 and 1 cGy of 1000 MeV/u iron ions, respectively (representative data in Figure 2, Panel A). The accumulation of 4-hydroxynonenal (HNE) adducts in proteins from the

same cultures indicates that increased lipid peroxidation was involved (representative data in Figure 2, Panel B). A 1.8 ± 0.2 (n=3) and 3.8 ± 1.4 (n=3) fold increases in proteins with 4-HNE adducts were detected at 24 h after exposure to 0.2 and 1 cGy of 1000 MeV/u iron ions, respectively.

The induction of stressful effects and their persistence, in low fluence-irradiated cell cultures, was further revealed when confluent cultures exposed to 1 cGy from 1000 MeV/u ^{56}Fe ions were subcultured to lower density (1:3) in fresh medium within 15 min after irradiation. Relative to control, increases in the levels of p-TP53ser15, p21^{Waf1} and HDM2 occurred at 8 and 24 h after subculture (Figure 3). Together, the magnitude of the various changes, in confluent and growing cell populations, suggests participation of a greater proportion of cells in the stress response than the 1.2-3.5 % fraction traversed by a primary particle track through the nucleus at a mean dose of 0.2 cGy. For example, for the 3.2 ± 1.0 (n=6)-fold-increases in p-TP53ser15 detected at 15 min, and 2.5 ± 0.3 fold (n=5)-increases in p21^{Waf1} levels detected at 3 h after exposure of cell cultures to 1 cGy of ^{56}Fe ions, to be solely due to effects in cells targeted through the nucleus by a primary ion, the cells would have to increase the level of these stress-responsive proteins by ~50-folds.

53BP1 foci formation in AG1522 cell cultures exposed to low fluences of HZE particles

To evaluate stressful effects in confluent cultures exposed to low fluences of HZE-particles on a cell by cell basis, we examined 53BP1 foci formation *in situ* at 15 min, 1 h, 3 h and 24 h after exposure to 0.2 cGy of either 1000 MeV/u ^{56}Fe ions, 600 MeV/u ^{28}Si ions or 3.7 MeV α particles. Separate cell cultures that received no radiation, but were sham-treated, were included for each time point and were considered

as respective controls (Figure 4). Whereas, only ~1.2-3.5 % of the cell nuclei are traversed by a primary HZE particle (Table 1), relative to respective control, the percent of cells with 53BP1 foci was increased at 15 min, 1 h and 3 h by 6.8 % (p <0.001), 15 % (p <0.001) and 10.6 % (p <0.001), respectively for ^{56}Fe ions (Figure 4, Panel A, experiment #1), and by 1.9 %, 7.7 % (p <0.001), and 5.3 % (p <0.001), respectively, for 3.7 MeV α particles (Figure 4, Panel B, experiment #1). Increases of 8.2 % (p <0.001), 11.4 % (p <0.001) and 2.8 % (p <0.05), at 15 min, 1 h and 3 h, respectively, were also observed after exposure to 0.2 cGy of ^{28}Si ions (Figure 4, Panel C, experiment #1). By 24 h, the percent increase of cells with 53BP1 foci was null for ^{56}Fe ions, was increased by 3.1 % (p <0.01) for ^{28}Si ions, and by 2 % for α particles (p <0.05). The significant increases in the excess percent of cells with foci (1.9–15 %) over what would be expected based on the percentage of cells irradiated through the nucleus (1.2-3.5 %) strongly support the participation of cells that were not targeted by the primary particle in the overall response of the cell population to irradiation by low fluences of high LET particles. Although the magnitude of the response varied between experiments, the trend was similar. At 1 h following irradiation by a mean absorbed dose of 0.2 cGy from iron ions, the increases in 53BP1 foci observed in experiments 2 and 3 were 10.3 % (p <0.001) and 7.3 % (p <0.001), respectively, compared to 15 % (p <0.001) in experiment 1 (Figure 4).

The fraction of cells with foci was shown to decrease by 2 h after exposure to DNA damaging agents (*23*). Thus, the increases observed at 1-3 h over those detected at 15 min in cultures exposed to ^{56}Fe ions or α particles could be due to recruitment of additional cells in the response. Presumably, these are bystander cells wherein signaling

molecules propagated from irradiated cells had time to exert effects that result in DNA damage. Whereas the attenuation of the percent increase of cells with 53BP1 foci at 24 h in iron ion- and α-particle-irradiated cells and at 3-24 h in silicon ion-irradiated cells may reflect repair of DNA damage in bystander cells, the persistent foci detected at these later times presumably reside in cells that were directly targeted by densely ionizing particles.

In contrast to ^{56}Fe ions (LET ~151 keV/μm), ^{28}Si ions (LET ~50 keV/μm) and α particles (LET ~109 keV/μm), exposure of confluent cultures to 0.2 cGy from 290 MeV/u ^{12}C ions (LET ~13 keV/um) did not result in significant increase in the percentage of cells with 53BP1 foci (not shown). This suggests that low mean absorbed doses of HZE particles with lower LET may be less efficient at inducing stressful effects (i.e. 53BP1 foci) under the conditions used in this study.

Cell culture system to identify cells irradiated with an HZE particle

Solid-state track detectors fused to cell culture dishes can be used to identify the position of primary HZE particle traversals. Experiments performed with such dishes suggested that the induction of stress in the form of 53BP1 foci is also observed in cells not traversed by primary HZE particles. We bonded a 100 μm-thick PADC solid state nuclear track detector (SSNTD) to the bottom edges of the cell culture surface (Supplementary Figure 1, Panel B). After etching of PADC plastic, cells that were likely traversed by a particle track could be identified, and induced biological effects may be assessed by suitable markers. The data in Figure 5 show 53BP1 foci in a confluent cell culture exposed to 0.2 cGy of 1000 MeV/u ^{56}Fe ions followed by 15 min incubation. Following cell fixation and etching of PADC, the iron ion tracks were visible as black dots (Figure 5, Panel A). Exposure to 0.2 cGy generally resulted in ~1.5 % of cells'

nuclei being superimposed on pits. The formation of 53BP1 foci (Figure 5, Panel B) in nuclei (revealed by DAPI staining, Figure 5, Panel C) that superimpose the black dots (inverted in white for better visualization, Figure 5, Panel D) indicates that these cells sustained DNA damage as would be expected from nuclear traversal by a high LET particle. The two cells with foci adjacent to the traversed cell are likely affected cells that were not targeted by the primary particle (Figure 5, Panel D). They may be bystander cells or cells subject to secondary radiations. The absence of SSNTD pits below these adjacent cells indicates lack of hot-spots; it suggests that the strategy of incorporating solid state nuclear track detector would be suitable for investigating the kinetics of biologic responses *in situ* in targeted and non-targeted cells.

The significance of secondary radiations in biological responses of cell cultures exposed to low fluence HZE particles

Secondary radiations resulting from the interaction of primary HZE particles with the target materials may have had a role in the apparent bystander effects. To shed additional light on this possibility, the contribution of secondary particles to the mean absorbed dose was calculated by simulations using the FLUKA multi-particle transport code (Table 2 and supplementary Tables 2-4). Estimates of the doses from heavy ions (primary and fragments), electrons, photons, protons and α particles to the AG1522 *cell monolayer* following exposure to a mean absorbed dose of 0.2 cGy from 1000 MeV/u ^{56}Fe ions, 600 MeV/u ^{28}Si ions or 290 MeV/u ^{12}C ions are described in Table 2. When exposed to any of the primary ions, secondary radiations consisting of HZE fragments, photons, protons and α particles, with a production threshold and a transport cut-off set at 1 keV, constituted <1 % of the total absorbed dose (Table 2). In contrast, electrons with a

production threshold set at 1 keV and transport cut-off set at 150 eV contributed ~37-40 % of the total dose. The mean absorbed dose deposited in the cell monolayer by HZE fragments was very small (0.0007 cGy, 0.0004 cGy and 0.0005 cGy following exposure to ^{56}Fe ions, ^{28}Si ions or ^{12}C ions, respectively) (Table 2). The dose contributed by photons, protons and α particles was minimal in all cases (Table 2).

Estimates of the mean absorbed doses to the glass cover-slip, cell monolayer and growth medium due to secondary radiations when the production threshold of δ rays was set at 1, 10 100 or 1000 keV and the transport cut off was set at 1 keV are described in Supplementary Tables 2-4. As the production threshold of the δ rays increased, the contribution of secondary electrons to the total mean absorbed dose delivered to the *cell monolayers* decreased and that of primary ions increased. Specifically, when the δ rays' production threshold was set at 1000 keV, the contribution of primary ions to the total mean absorbed dose to a *cell monolayer* exposed to 1000 MeV/u ^{56}Fe ions increased to ~97 % and that of electrons decreased to ~2 % (supplementary Table 2). In case of 600 MeV/u ^{28}Si ions and 290 MeV/u ^{12}C ions, the secondary electrons represented, respectively, 0.96 % and almost nil of the total mean absorbed dose to the *cell monolayer* (Supplementary Tables 3 and 4).

Quantifying the radial distribution of the secondary particles is essential before attributing stressful effects, observed in cells that surround directly targeted cells to a bystander effect. The data in Figure 6 represent the radial dose distributions (heavy ions, electrons and the total dose) in a 1 μm-thick cell culture layer exposed to an orthogonal narrow beam of 1000 MeV/u ^{56}Fe ions. Panel A shows that the heavy ions deposit their energy mainly in the first 10 μm, while the electron dose extends out to ~100 μm radius

around the track of the primary ion. Panel B describes the radial distribution of dose from δ rays with 1-, 10-, 100 or 1000 keV-production-thresholds. Panels C and D permit visualization of the radial dose deposited by heavy ions or electrons, respectively, around the primary track pit revealed by etching of PADC and staining nuclei with DAPI as described in Figure 5 (Panel D). It is noteworthy that the magnitude of the total radial dose distribution, calculated in our studies, is in accord with previous results (*51*).

In the FLUKA code, the ionization energy losses are processed as continuous energy loss or as discrete ionization events. Above the pre-set threshold, the ionization is modeled as production of δ rays, based on scattering of the projectile with a free electron. This threshold of δ ray production is an important parameter in this type of simulation. At radial distances less than 20 μm from the track, the calculated absorbed dose depends strongly on the threshold value (1, 10 or 100 keV) (Figure 6, Panel B). As expected, low thresholds should be used to accurately simulate radial dose distributions around the track core with μm and sub-μm spatial resolution (*52*).

The data in Figure 6 therefore imply that, in our experiments, the chance for heavy fragments to hit neighboring cells is negligible. However, this is not the case for secondary electrons which can travel significant distances from the track. Energy deposition by δ rays is a stochastic process, and the possibility exists that some cells in the vicinity of cells targeted by a primary ion may receive a biologically relevant dose.

DISCUSSION

The lack of clear knowledge about non-targeted responses has been singled out by the US National Academies (*53*) as one of the important factors limiting the prediction of radiation health risks associated with space exploration. During deep space missions,

every cell nucleus in an astronaut's body would be hit by a proton or secondary electron every few days and by an HZE ion about once a month (*54*); the rest would be bystanders. Human epidemiological studies would be ideal to predict the health risks of exposure to low fluences of space particulate radiations; however, given the relatively insignificant number of humans exposed to such radiations, mechanistic studies in cell culture systems and animals are critical to help estimate corresponding risks to humans.

Using molecular, biochemical, physical and computational approaches, here we provide evidence for the amplification of HZE-particle-induced stressful effects in normal human fibroblast cultures following exposure to doses as low as 0.2 cGy of 1000 MeV/u iron ions or 600 MeV/u silicon ions (Figures 1-5). Consistent with previous results in cell cultures exposed to low fluences of α particles, another type of radiation with similar quality (i.e. high LET character), increases in the levels of proteins that participate in TP53 and ERK1/2 signaling pathways (*55*) were observed. These increases were detected as early as 15 min after irradiation and persisted for at least 24 h. Relative to control, higher levels of p-TP53ser15, a marker of DNA damage, was detected in confluent AG1522 fibroblasts exposed to a mean absorbed dose of 0.2 cGy that targets, on average, only 1-3 % of the cells through the nucleus. This was associated 1-3 h later (Figure 1, Panels B and C) with increased level of $p21^{Waf1}$, a p53 effector and key component of the DNA damage induced G_1 checkpoint. The induction of these stress markers persisted for at least 24 h (Figure 1, Panel D) and was associated with an increase in protein carbonylation and in accumulation of 4-HNE protein adducts (Figure 2, Panels A and B). Interestingly, 4-HNE reactive aldehydes originate from peroxidation of membrane lipids where key proteins that mediate stress-induced

bystander effects, including connexins, cyclooxygenase-2 and NAD(P)H oxidase, reside (*56*). The accumulation of such protein adducts may modulate transport properties of the plasma membrane, gene expression, including signal transduction pathways affecting DNA damage sensing and repair, cell survival and cell proliferation (*57*). The occurrence of such appreciable oxidative effects, long after exposure, is consistent with excess ROS generation due to perturbations in oxidative metabolism and/or persistent activation of oxidases (*58, 59*). It suggests the involvement of a greater fraction of cells than those targeted by a primary particle in the overall response leading to oxidative stress. Whereas the persistence of stress may be due to sustained changes in the targeted and non-targeted cells that were affected early after exposure, it could also result from induction of stress in additionally recruited cells that were not-targeted by a primary particle. This does not preclude, however, the restitution of damage and return to the basal state in certain affected non-targeted and targeted cells.

The DNA DSB is a serious threat to the integrity of eukaryotic genomes (*60*). Following exposure to DNA damaging agents, a battery of damage sensing and repair proteins localize at the site of DNA breaks. Among these proteins, 53BP1 forms discrete foci within minutes after exposure (*23, 46, 61*). Here, we used the formation of 53BP1 foci as a biomarker to investigate the evolution of α- and HZE-particle-induced propagation of signaling events leading to DNA damage in cells that were not targeted by a primary particle. We used the same microscope optics and exposure time, and scored by eye to accurately differentiate foci; we also used separate controls for each time point. Utilizing these criteria, the results from cultures exposed to a dose by which only 1-3 % of cells are traversed through the nucleus by a primary energetic ion strongly supported

the participation of cells other than those targeted by the primary particles in the response. At 15 min after exposure to 0.2 cGy from α particles, ^{56}Fe ions or ^{28}Si ions, the fraction of cells with 53BP1 foci was higher than predicted based on the percentage of nuclei directly targeted by primary ions (Figure 4). Whereas secondary radiation may have contributed to the effects observed in the HZE-particle irradiated cell cultures, this cannot be the case in the studies using our α particle irradiator. The ranges of δ rays produced by the interaction of these α particles (3.7 MeV, 0.5 MeV FWHM) with the cells are very small compared with the nuclear diameter. Hence, the effects observed in α-particle-irradiated cell cultures (Figure 4) clearly support the spread of stressful effects to unirradiated bystander cells.

In general, it is thought that 53BP1 foci formation is transient. Following uniform exposure of cell cultures to an absorbed dose of 1 Gy from ^{137}Cs γ rays, the fraction of cells with foci peaked at 20 min and remained elevated for 2 h after irradiation; it decreased exponentially and returned to basal level 16 h later (*23*). In our study with cell cultures where only 1.2-3.5 % of nuclei were irradiated with α particles, iron ions or silicon ions, the maximum increase in the fraction of cells with 53BP1 foci was detected at 1 h. The persistent elevation in foci formation at 3 h may be due to the induction of DNA damage in non-directly targeted cells. At 3 h after exposure, foci formation in iron ion- and α-particle-irradiated cultures was increased not only over control but also compared to cultures examined at 15 min after irradiation (p <0.001). Whereas, the increases in the fraction of cells with foci at 1 and 3 h may reflect the spread of stressful effects to additional cells than those targeted by radiation, they may also reflect

development of foci in affected cells (irradiated and bystander) that required time to become visible by microscopy.

In contrast to ^{56}Fe ions, ^{28}Si ions and α particles, no excess 53BP1 foci formation has been detected after exposure of cell cultures to 0.2 cGy from 290 MeV/u carbon ions (LET ~13 keV/μm) at any time between 15 min and 24 h after irradiation. This may be due to less complex DNA damage being induced in the targeted cells, which may affect the nature of the propagated signaling events. At a mean absorbed dose of 0.2 cGy to the exposed cultures from 290 MeV/u carbon ions, ~0.015 cGy are deposited in the nucleus from a single particle traversal; in comparison, ~17.25 cGy, 5.7 cGy and 12.45 cGy are deposited by single traversals of 1000 MeV/u Fe, 600 MeV/u silicon and 3.7 MeV α particles[2], respectively. Thus, the dose absorbed by the targeted nuclei likely plays an important role in the induction of stressful effects leading to DNA damage. Different targeted and non-targeted effects may however occur following cellular hits with multiple carbon ions. The use of microbeams would greatly facilitate such experiments and would be informative of the effects of absorbed dose and radiation quality.

Culture dishes that incorporate nuclear track etch detectors were developed in order to identify cells and cell nuclei traversed by primary HZE particles. Our preliminary experiments suggest that the induction of stress in the form of 53BP1 foci is also observed in cells that were not traversed by a primary ^{56}Fe ion. The strategy of using culture dishes with nuclear track detector to examine biological changes in HZE-particle-irradiated cultures expanded our previous studies with α particles (*34*), and permitted irradiation of cell cultures grown in dishes with sealable-lid in presence of pH-

[2] The absorbed dose (d) per traversal to the thin disk-shaped cell nucleus of the AG1522 cell was calculated according to the relation $d = (0.16\ \mathrm{LET})/(A\ \rho)$, where A is the cross-sectional area of the cell nucleus (i.e. an average of ~140 μm^2), and ρ is the density of the cell.

equilibrated culture medium with a horizontal broadbeam. Time-course experiments using these dishes, together with determination of the metrology of distance propagation as we have previously done with low fluence α-particle-irradiated cell cultures (*34*), would be highly informative of the kinetics of induction and decay of biological changes in cell cultures exposed to low fluences of HZE particle. In such studies careful characterization of the positional accuracy of the primary track is essential. A typical 10 μm spatial deviation may have to be considered due to scattering of the incident ion as it crosses the polymer material of the nuclear track etch detector.

To evaluate the possibility of whether the stressful effects expressed in presumed bystander cells in low fluence HZE-particle-irradiated cultures may be due to secondary particles generated from fragmentation of the incident beam in the target material (Table 2, Supplementary Tables 2-4), we performed computational simulations using the FLUKA multi-particle transport code. The capabilities of this code have been demonstrated in simulations for microdosimetric purposes and tissue equivalent proportional counters (*51, 62*). Our simulations showed that, using glass-bottomed flaskettes, the total dose to the monolayer due to HZE fragments is negligible. Importantly, the radial dose due to these fragments is confined to ~10 μm around the primary track. In contrast, the dose due to δ rays may be substantial. Depending on energy, the range of the δ rays can be extensive (e.g., ~130 μm for 100 keV δ rays) (*63, 64*), thus likely targeting all cells in the exposed culture (Figure 6). Whereas, the biological effects induced by δ rays may be stressful, they can also attenuate damaging effects propagated from cells targeted with primary and HZE fragments. In case of cells exposed to 3.7 MeV α particles, the complications in interpreting the apparent bystander

effects (Figures 1 and 4) are diminished, as these particles do not produce secondary radiation that cross-irradiate neighboring cells (*26*).

Experimental systems that allow deciphering the nature of biological effects due to δ rays and to the primary HZE fragments would be highly informative towards understanding the spectrum of biological changes induced following exposure to low fluences of HZE particles. In this context, co-culture systems that allow investigation of HZE-particle-induced non-targeted effects in the absence of secondary fragmentation products, or δ rays, generated strong evidence for the propagation from irradiated cells of signaling events leading to oxidative stress and DNA damage in bystander cells, an effect that persisted in their progeny (*18*). Importantly, the expansion of HZE-particle-induced non-targeted effects to *in vivo* systems (*65*), together with characterization of the magnitude of effects due to fragmentation products, the modulating effect of δ rays, and of the underlying mechanisms, is of importance to human space exploration and hadron therapy (*66*). In particular, exposure of biological specimens at very low dose-rate to simulate more closely the doses received during space travel (*54*) would be essential. During a 24 h period, these doses are significantly lower than the lowest dose of 0.2 cGy used in our studies.

CONCLUSION

The data reported here highlight the manifestation of stressful effects in confluent normal human cell cultures exposed to low fluences of HZE particles by several endpoints. The results show that propagation of the signaling events leading to stressful effects in cells not targeted by a primary particle is rapid, but the reaction to the propagated signal(s) may require time to be expressed depending on the endpoint

investigated. The phenotype (e.g. redox environment) of both, the signal emitting cells and the recipient cells may greatly affect the kinetics of expression of biological changes. Indeed, studies have shown that the DNA repair capacity of non-targeted cells (*67, 68*), their anti-oxidant potential (*69*), and their genotype (*70*) modulate bystander effects. The results with 53BP1 foci formation showed that by 24 h after exposure to 1000 MeV/u ^{56}Fe ions, the excess formation of foci was greatly reduced. This may suggest that the induction of DNA damage in presumed bystander cells is transient; however, accumulating data from experiments involving co-cultures of HZE-particle-irradiated cells with unirradiated bystander cells show that the latter experience genomic instability that manifests in perturbations in oxidative metabolism (*18*) and excess chromosomal damage in their progeny (*11, 19*).

Additional FLUKA calculations to determine both the fraction of cells that were not targeted by fragmentation products and the fraction of cells that were hit by these products together with the doses received are necessary to enhance our understanding of low fluences HZE particle- induced bystander effects. This approach will require a different model, with individual cells being considered under the same experimental conditions. Depending on cell culture conditions (e.g. glass versus polystyrene platform for cell growth, thickness of platform, cell thickness etc.) the yield and nature of fragmentation products may vary, which may impact the signaling pathways leading to enhancement or attenuation of stressful effects expressed in the exposed cell cultures. The physical and physico-chemical events resulting from irradiation with primary or secondary fragments (*71-73*), including yield, lifetime and spatial distribution of the generated radiolytic species may induce prominent biochemical and genetic changes that

affect intercellular communication between irradiated and bystander cells, which may modulate the magnitude of the induced stress response and determine long-term biological effects. Together, these studies may greatly contribute to the efforts by NASA to develop risk based radiation exposure guidelines that minimize adverse health effects in astronauts.

ACKNOWLEDGMENTS

We thank Dr. Peter Guida and his team at the NASA Space Radiation Laboratory for their support during the experiments. We are grateful to Drs. Adam Rusek, Michael Sivertz and I-Hung Chang for dosimetry support. We thank Drs. Hatsumi Nagasawa, Les Braby and John Ford for their gift of polyethylene terephthalate. We also thank Gary Moss from Track Analysis Systems Ltd. for his input in developing the dishes with Tastrak™-bottom. The input of Manuela Buonanno, Narongchai Autsavapromporn and Jie Zhang in the course of the experiments is greatly appreciated. This research was supported by NASA Grant NNJ06HD91G and by Grant CA049062 from the National Institute of Health; RWH is supported by grant CA83838 from the National Institute of Health.

REFERENCES

1. Little JB. Genomic instability and bystander effects: a historical perspective. Oncogene 2003; 22:6978-87.

2. Nagasawa H, Little JB. Induction of sister chromatid exchanges by extremely low doses of α-particles. Cancer Res 1992; 52:6394-6.

3. Nagasawa H, Little JB. Unexpected sensitivity to the induction of mutations by very low doses of alpha-particle irradiation: Evidence for a bystander effect. Radiat Res 1999; 152:552-7.

4. Zhou H, Randers-Pehrson G, Waldren CA, Vannais D, Hall EJ, Hei TK. Induction of a bystander mutagenic effect of alpha particles in mammalian cells. Proc Natl Acad Sci USA 2000; 97:2099-104.

5. Ponnaiya B, Jenkins-Baker G, Bigelow A, Marino S, Geard CR. Detection of chromosomal instability in alpha-irradiated and bystander human fibroblasts. Mutat Res 2004; 568:41-8.

6. Azzam EI, de Toledo SM, Little JB. Direct evidence for the participation of gap-junction mediated intercellular communication in the transmission of damage signals from alpha-particle irradiated to non-irradiated cells. Proc Natl Acad Sci USA 2001; 98:473-8.

7. Azzam EI, de Toledo SM, Gooding T, Little JB. Intercellular communication is involved in the bystander regulation of gene expression in human cells exposed to very low fluences of alpha particles. Radiat Res 1998; 150:497-504.

8. Hickman AW, Jaramillo RJ, Lechner JF, Johnson NF. Alpha-particle-induced p53 protein expression in a rat lung epithelial cell strain. Cancer Res 1994; 54:5797-800.

9. Sowa MB, Goetz W, Baulch JE, Pyles DN, Dziegielewski J, Yovino S, et al. Lack of evidence for low-LET radiation induced bystander response in normal human fibroblasts and colon carcinoma cells. Int J Radiat Biol 2010; 86:102-13.

10. Sawant SG, Randers-Pehrson G, Geard CR, Brenner DJ, Hall EJ. The bystander effect in radiation oncogenesis: I. Transformation in C3H 10T1/2 cells in vitro can be initiated in the unirradiated neighbors of irradiated cells. Radiat Res 2001; 155:397-401.

11. Buonanno M, de Toledo SM, Azzam EI. Increased frequency of spontaneous neoplastic transformation in progeny of bystander cells from cultures exposed to densely-ionizing radiation. PloS one 2011; 6: art. no. e21540.

12. Shao C, Furusawa Y, Kobayashi Y, Funayama T, Wada S. Bystander effect induced by counted high-LET particles in confluent human fibroblasts: a mechanistic study. FASEB J 2003; 17:1422-7.

13. Hamada N, Ni M, Funayama T, Sakashita T, Kobayashi Y. Temporally distinct response of irradiated normal human fibroblasts and their bystander cells to energetic heavy ions. Mutat Res 2008; 639:35-44.

14. Harada K, Nonaka T, Hamada N, Sakurai H, Hasegawa M, Funayama T, et al. Heavy-ion-induced bystander killing of human lung cancer cells: role of gap junctional intercellular communication. Cancer Sci 2009; 100:684-8.

15. Fournier C, Becker D, Winter M, Barberet P, Heiss M, Fischer B, et al. Cell cycle-related bystander responses are not increased with LET after heavy-ion irradiation. Radiat Res 2007; 167:194-206.

16. Yang H, Anzenberg V, Held KD. The time dependence of bystander responses induced by iron-ion radiation in normal human skin fibroblasts. Radiat Res 2007; 168:292-8.

17. Yang H, Anzenberg V, Held KD. Effects of heavy ions and energetic protons on normal human fibroblasts. Radiatsionnaia biologiia, radioecologiia / Rossiiskaia akademiia nauk 2007; 47:302-6.

18. Buonanno M, De Toledo SM, Pain D, Azzam EI. Long-term consequences of radiation-induced bystander effects depend on radiation quality and dose and correlate with oxidative stress. Radiat Res 2011; 175:405-15.

19. Ponnaiya B, Suzuki M, Tsuruoka C, Uchihori Y, Wei Y, Hei TK. Detection of chromosomal instability in bystander cells after Si490-ion irradiation. Radiat Res 2011; 176:280-90.

20. Groesser T, Cooper B, Rydberg B. Lack of bystander effects from high-LET radiation for early cytogenetic end points. Radiat Res 2008; 170:794-802.

21. Fournier C, Barberet P, Pouthier T, Ritter S, Fischer B, Voss KO, et al. No evidence for DNA and early cytogenetic damage in bystander cells after heavy-ion microirradiation at two facilities. Radiat Res 2009; 171:530-40.

22. Cucinotta FA, Chappell LJ. Non-targeted effects and the dose response for heavy ion tumor induction. Mutat Res 2010; 687:49-53.

23. Schultz LB, Chehab NH, Malikzay A, Halazonetis TD. p53 binding protein 1 (53BP1) is an early participant in the cellular response to DNA double-strand breaks. J Cell Biol 2000; 151:1381-90.

24. Goodhead DT. The initial physical damage produced by ionizing radiations. Int J Radiat Biol 1989; 56:623-34.

25. Ponomarev AL, Cucinotta FA. Nuclear fragmentation and the number of particle tracks in tissue. Radiat Prot Dosimetry 2006; 122:354-61.

26. Hamm RN, Turner JE, Ritchie RH, Wright HA. Calculation of heavy-ion tracks in liquid water. Radiat Res 1985; 104:S20-S6.

27. Cucinotta F, Nikjoo H, Goodhead DT. The effect of delta rays on the number of particle traversals per cell in laboratory and space exposures. Radiat Res 1998; 150:115-19.

28. Metting NF, Rossi HH, Braby LA, Kliauga PJ, Howard J, Zaider M, et al. Microdosimetry near the trajectory of high-energy heavy ions. Radiat Res 1988; 116:183-95.

29. Elmore E, Lao XY, Kapadia R, Redpath JL. Threshold-type dose response for induction of neoplastic transformation by 1 GeV/nucleon iron ions. Radiat Res 2009; 171:764-70.

30. Aiginger H, Andersen V, Ballarini F, Battistoni G, Campanella M, Carboni M, et al. The FLUKA code: new developments and application to 1 GeV/n iron beams. Adv Space Res 2005; 35:214-22.

31. Battistoni G, Muraro S, Sala PR, Cerutti F, Ferrari A, Roesler S, et al., The FLUKA code: Description and benchmarking. In *Proceedings of the Hadronic Shower Simulation Workshop 2006* (A. Albrow RR, Ed.), pp. 31-49. AIP Conference Proceeding, Fermilab, 2007.

32. FLUKA: A Multi-Particle Transport Code. Geneva: CERN European organization for nuclear research; 2005.

33. Terasima T, Tolmach LJ. Changes in x-ray sensitivity of HeLa cells during the division cycle. Nature 1961; 190:1210-11.

34. Gaillard S, Pusset D, de Toledo SM, Fromm M, Azzam EI. Propagation distance of the alpha-particle-induced bystander effect: the role of nuclear traversal and gap junction communication. Radiat Res 2009; 171:513-20.

35. Gray LH, Conger AD, Ebert M, Hornsey S, Scott OC. The concentration of oxygen dissolved in tissues at the time of irradiation as a factor in radiotherapy. Br J Radiol 1953; 26:638-48.

36. Rueckert RR, Mueller GC. Effect of oxygen tension on HeLa cell growth. Cancer Res 1960; 20:944-9.

37. Neti PV, de Toledo SM, Perumal V, Azzam EI, Howell RW. A multi-port low-fluence alpha-particle irradiator: fabrication, testing and benchmark radiobiological studies. Radiat Res 2004; 161:732-8.

38. Charlton DE, Sephton R. A relationship between microdosimetric spectra and cell survival for high-LET irradiation. Int J Radiat Biol 1991; 59:447-57.

39. Cucinotta FA, Katz R, Wilson JW. Radial distribution of electron spectra from high-energy ions. Radiat Environ Biophys 1998; 37:259-65.

40. FLUKA. Version 2011.2.12. Battistoni G, Broggi F, Brugger M, Campanella M, Carboni M, Empl A, et al. 2011.

41. Cornforth MN, Schillaci ME, Goodhead DT, Carpenter SG, Wilder ME, Sebring RJ, et al. Radiobiology of ultrasoft X rays. III. Normal human fibroblasts and the significance of terminal track structure in cell inactivation. Radiat Res 1989; 119:511-22.

42. Woodard HQ, White DR. The composition of body tissues. Br J Radiol 1986; 59:1209-18.

43. Stadtman ER. Oxidation of free amino acids and amino acid residues in proteins by radiolysis and by metal-catalyzed reactions. Annu Rev Biochem 1993; 62:797-821.

44. Voulgaridou GP, Anestopoulos I, Franco R, Panayiotidis MI, Pappa A. DNA damage induced by endogenous aldehydes: current state of knowledge. Mutat Res 2011; 711:13-27.

45. Romero-Calvo I, Ocon B, Martinez-Moya P, Suarez MD, Zarzuelo A, Martinez-Augustin O, et al. Reversible Ponceau staining as a loading control alternative to actin in Western blots. Anal Biochem 2010; 401:318-20.

46. Rappold I, Iwabuchi K, Date T, Chen J. Tumor suppressor p53 binding protein 1 (53BP1) is involved in DNA damage-signaling pathways. J Cell Biol 2001; 153:613-20.

47. Wilson PF, Nham PB, Urbin SS, Hinz JM, Jones IM, Thompson LH. Inter-individual variation in DNA double-strand break repair in human fibroblasts before and after exposure to low doses of ionizing radiation. Mutat Res 2010; 683:91-7.

48. Ugenskiene R, Prise K, Folkard M, Lekki J, Stachura Z, Zazula M, et al. Dose response and kinetics of foci disappearance following exposure to high- and low-LET ionizing radiation. Int J Radiat Biol 2009; 85:872-82.

49. Canman CE, Lim DS, Cimprich KA, Taya Y, Tamai K, Sakaguchi K, et al. Activation of the ATM kinase by ionizing radiation and phosphorylation of p53. Science 1998; 281:1677-9.

50. Valerie K, Yacoub A, Hagan MP, Curiel DT, Fisher PB, Grant S, et al. Radiation-induced cell signaling: inside-out and outside-in. Molecular Can Ther 2007; 6:789-801.

51. Bohlen TT, Dosanjh M, Ferrari A, Gudowska I, Mairani A. FLUKA simulations of the response of tissue-equivalent proportional counters to ion beams for applications in hadron therapy and space. Phys Med Biol 2011; 56:6545-61.

52. Bohlen TT, Cerutti F, Dosanjh M, Ferrari A, Gudowska I, Mairani A, et al. Benchmarking nuclear models of FLUKA and GEANT4 for carbon ion therapy. Phys Med Biol 2010; 55:5833-47.

53. Managing Space Radiation Risk in the New Era of Space Exploration. Washington, D.C.: The National Academies Press; 2008.

54. Cucinotta F, Durante M. Cancer risk from exposure to galactic cosmic rays: implications for space exploration by human beings. Lancet Oncol 2006; 7:431-5.

55. Azzam EI, de Toledo SM, Little JB. Oxidative metabolism, gap junctions and the ionizing radiation-induced bystander effect. Oncogene 2003; 22:7050-7.

56. Anderson RG, Jacobson K. A role for lipid shells in targeting proteins to caveolae, rafts, and other lipid domains. Science 2002; 296:1821-5.

57. Poli G, Schaur RJ, Siems WG, Leonarduzzi G. 4-hydroxynonenal: a membrane lipid oxidation product of medicinal interest. Med Res Rev 2008; 28:569-631.

58. Petkau A. Role of superoxide dismutase in modification of radiation injury. Br J Cancer Suppl 1987; 8:87-95.

59. Spitz DR, Azzam EI, Li JJ, Gius D. Metabolic oxidation/reduction reactions and cellular responses to ionizing radiation: a unifying concept in stress response biology. Cancer Metastasis Rev 2004; 23:311-22.

60. Iliakis G. The role of DNA double strand breaks in ionizing radiation-induced killing of eukaryotic cells. Bioessays 1991; 13:641-8.

61. Asaithamby A, Uematsu N, Chatterjee A, Story MD, Burma S, Chen DJ. Repair of HZE-particle-induced DNA double-strand breaks in normal human fibroblasts. Radiat Res 2008; 169:437-46.

62. Northum JD, Guetersloh SB, Braby LA. FLUKA capabilities for microdosimetric analysis. Radiat Res 2012; 177:117-23.

63. Hamm RN, Wright HA, Katz R, Turner JE, Ritchie RH. Calculated yields and slowing-down spectra for electrons in liquid water: implications for electron and photon RBE. Phys Med Biol 1978; 23:1149-61.

64. Howell RW. Radiation spectra for Auger-electron emitting radionuclides: Report No. 2 of AAPM Nuclear Medicine Task Group No. 6. Med Phys 1992; 19:1371-83.

65. Jain MR, Li M, Chen W, Liu T, De Toledo SM, Pandey BN, et al. In vivo space radiation-induced non-targeted responses: late effects on molecular signaling in mitochondria. Curr Mol Pharmacol 2011; 4:106-14.

66. Blakely EA. New measurements for hadrontherapy and space radiation: biology. Phys Med 2001; 17 Suppl 1:50-8.

67. Little JB, Nagasawa H, Li GC, Chen DJ. Involvement of the nonhomologous end joining DNA repair pathway in the bystander effect for chromosomal aberrations. Radiat Res 2003; 159:262-7.

68. Mothersill C, Seymour RJ, Seymour CB. Bystander effects in repair-deficient cell lines. Radiat Res 2004; 161:256-63.

69. Azzam EI, de Toledo SM, Spitz DR, Little JB. Oxidative metabolism modulates signal transduction and micronucleus formation in bystander cells from alpha-particle-irradiated normal human fibroblast cultures. Cancer Res 2002; 62:5436-42.

70. Lorimore SA, Chrystal JA, Robinson JI, Coates PJ, Wright EG. Chromosomal instability in unirradiated hemaopoietic cells induced by macrophages exposed in vivo to ionizing radiation. Cancer Res 2008; 68:8122-6.

71. Cucinotta FA, Plante I, Ponomarev AL, Kim MH. Nuclear interactions in heavy ion transport and event-based risk models. Radiat Prot Dosimetry 2011; 143:384-90.

72. Meesungnoen J, Jay-Gerin J-P, Radiation chemistry of liquid water with heavy ions: Monte Carlo simulation studies. In *Charged Particle and Photon Interactions with Matter Recent Advances, Applications, and Interfaces* (Hatano Y, Katsumura YMozumder A, Eds.), pp. 355-400. Taylor and Francis, Boca Raton, FL, 2011.

73. Turner JE, Magee JL, Wright HA, Chatterjee A, Hamm RN, Ritchie RH. Physical and chemical development of electron tracks in liquid water. Radiat Res 1983; 96:437-49.

FIGURE LEGENDS

Figure 1. Western blot analyses of p-TP53ser15, p-ERK1/2, $p21^{Waf1}$ and HDM2 in AG1522 cell populations at [A] 15 min, [B] 1 h, [C] 3 h, [D] 6 and 24 h after exposure to an absorbed dose of 0, 0.2 or 1 cGy from 1000 MeV/u ^{56}Fe ions, 600 MeV/u ^{28}Si ions or 3.7 MeV α particles. Staining with Ponceau S Red was used as loading control. Each immunoblot is representative of 2-7 experiments. Fold change represents relative change compared to the control (i.e. 0 cGy).

Figure 2. Oxidative stress in confluent AG1522 cells harvested 24 h after exposure to low mean absorbed doses of 1000 MeV/u ^{56}Fe ion. Immunoblot analyses of [A] protein carbonylation, and [B] lipid peroxidation (measured by 4-HNE protein adduct accumulation). In the case of protein carbonylation, the relative intensity (i.e. fold-change) in oxidation of the overall spectrum of proteins (~30-130 kDa) in irradiated cells was compared to that in control cells. For 4-HNE protein adduct accumulation, the relative intensity refers to the level of the band with arrow relative to control. Staining with Ponceau S Red was used as loading control. Each immunoblot is representative of 3 experiments.

Figure 3. Western blot analyses of $p21^{Waf1}$, p-TP53ser15 and HDM2 in AG1522 cell populations exposed to 1000 MeV/u ^{56}Fe ions. Confluent cells were exposed to a mean absorbed dose of 1 cGy and subcultured in fresh medium (1:3). Samples were harvested for analyses 8 and 24 h after irradiation. Staining with Ponceau S Red was used as loading control. Each immunoblot is representative of 3-5 experiments. Fold change represents relative change compared to the control.

Figure 4. Kinetics of 53BP1 foci formation in confluent AG1522 cell cultures exposed to 0.2 cGy from 1000 MeV/u ^{56}Fe ions (Panel A), 3.7 MeV α particles (Panel B) or 600 MeV/u ^{28}Si ions (Panel C). The data represent the excess percent increase (ΔF) of cells with 53BP1 foci in irradiated cell populations relative to the respective control calculated as $\Delta F = 100 (F_{irradiated} - F_{control})$ where F is the ratio of the number of cells with 53BP1 foci over the total number of cells counted. Each graph is representative of 3 different experiments. χ^2 test was performed on the total number of cells compared with respective control in irradiated populations . (*: $p < 0.05$; **: $p < 0.01$; ***: $p < 0.001$).

Figure 5. Representative images of etched tracks and 53BP1 foci in AG1522 cell cultures grown on dishes with CR-39-nuclear track detector bottom. The cultures were fixed for analyses at 15 min after exposure to 0.2 cGy of 1000 MeV/u ^{56}Fe ions: (A) visualization of etched tracks; (B) 53BP1 immuno-detection (red); (C) stained with DAPI; (D) images in A-C are super-imposed with the black dots representing etched tracks in (A) converted to white for better visualization.

Figure 6. FLUKA simulation of radial distribution of dose, per primary irradiating particle, in 1 μm-thick cell culture layer exposed to 0.2 cGy of 1000 MeV/u ^{56}Fe ions. [A] Radial distribution of dose of ^{56}Fe ions, heavy ions, 1 keV-threshold electrons and the total dose. [B] Radial distribution of dose of electrons with various δ ray-thresholds (1, 10 and 100 keV and 1 MeV). Panels [C] and [D] illustrate radial distribution of dose from heavy ions (primary and secondary) and electrons, respectively, by superimposing the radial dose area over Panel D in Figure 5, where cells traversed by a primary ^{56}Fe ion-track were identified.

Supplementary Figure 1. Schematics of tissue culture systems used in experiments. [A] Glass-bottomed flaskette (Nalge Nunc International). [B] Tissue culture dish with polyallyl diglycol carbonate (PADC, commonly known as Columbia Resin #39) plastic polymer bottom for HZE-particle-irradiation. Incorporation of a 100 μm-thick PADC film below the glass bottom of the sealable-dish permits visualization of HZE-particle-tracks without interfering with microscopic examination of biological changes. The dishes filled to capacity with pH- and temperature-equilibrated growth medium can be positioned perpendicularly to the incident beam.

FOOTNOTES

[1] The thickness of ~1 μm of an AG1522 cell (*41*) was estimated from studies in fixed/dehydrated cells grown on Mylar. The actual dimension of a live AG1522 cell grown on glass may be different.

[2] The absorbed dose (d) per traversal to the thin disk-shaped cell nucleus of the AG1522 cell was calculated according to the relation $d = (0.16\ \mathrm{LET})/(A\ \rho)$, where A is the cross-sectional area of the cell nucleus (i.e. an average of ~140 μm^2), and ρ is the density of the cell.

In confluent cell cultures

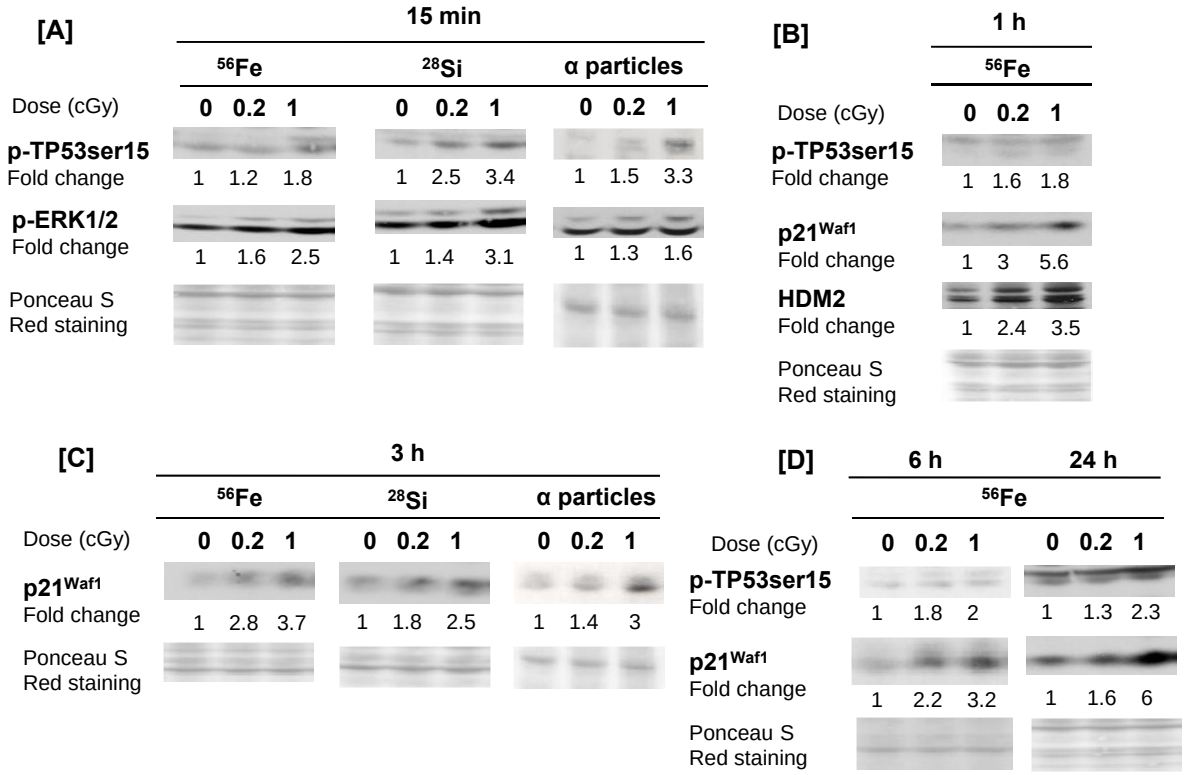

In confluent cell cultures

Oxidative Stress Dose Response to ^{56}Fe ions

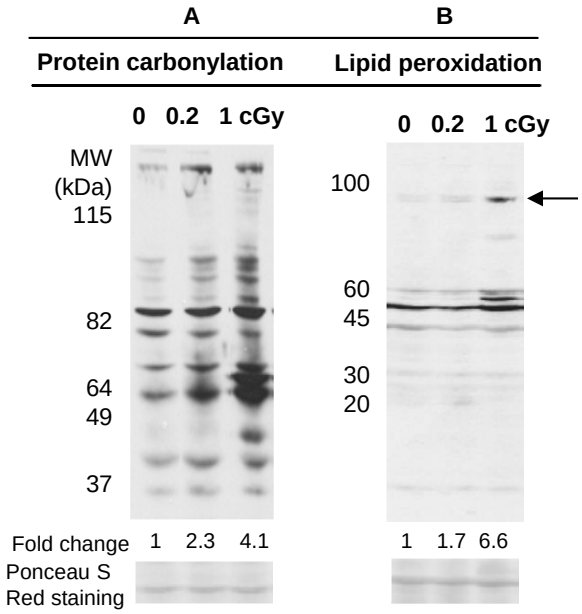

In proliferating cells

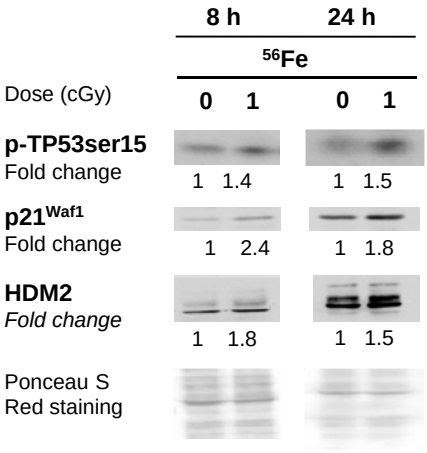

[A] 1000 MeV/u ^{56}Fe ions (LET ~151 keV/µm)

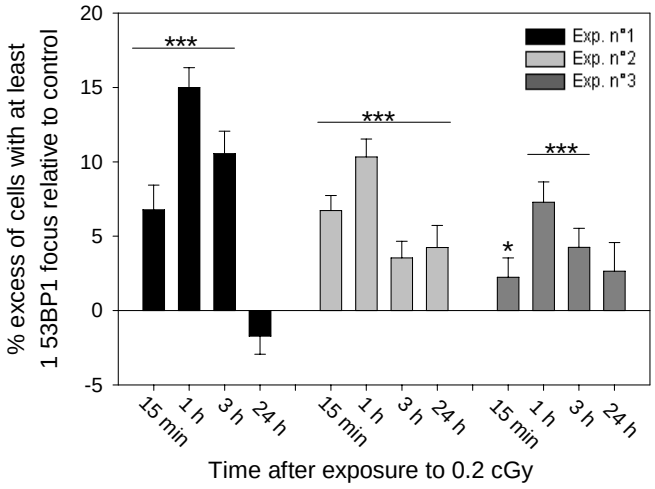

[B] 3.7 MeV α particles (LET ~109 keV/µm)

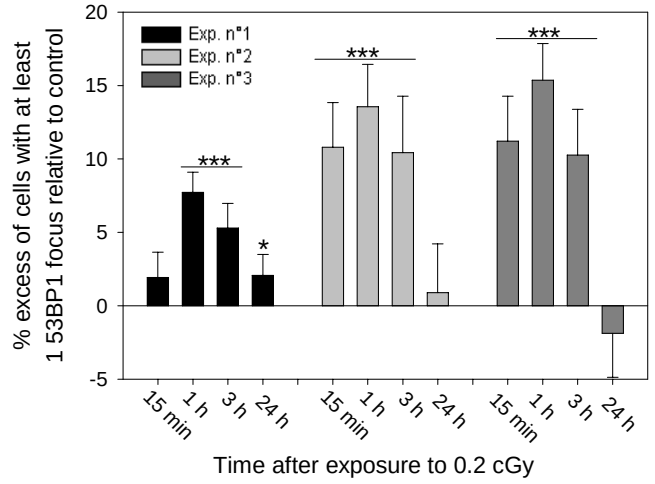

[C] 600 MeV/u ^{28}Si ions (LET ~50 keV/µm)

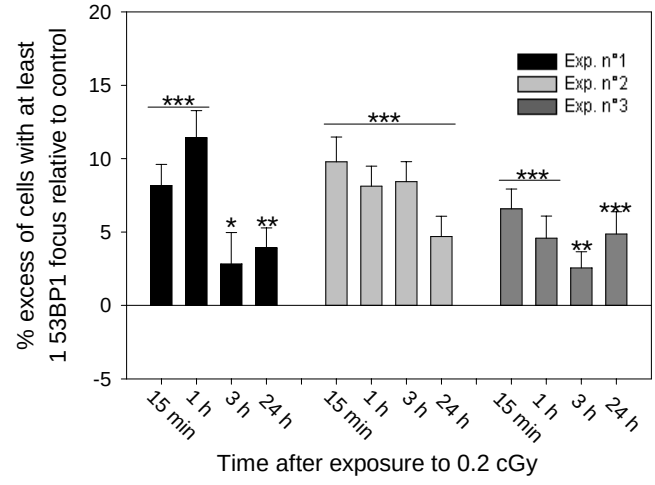

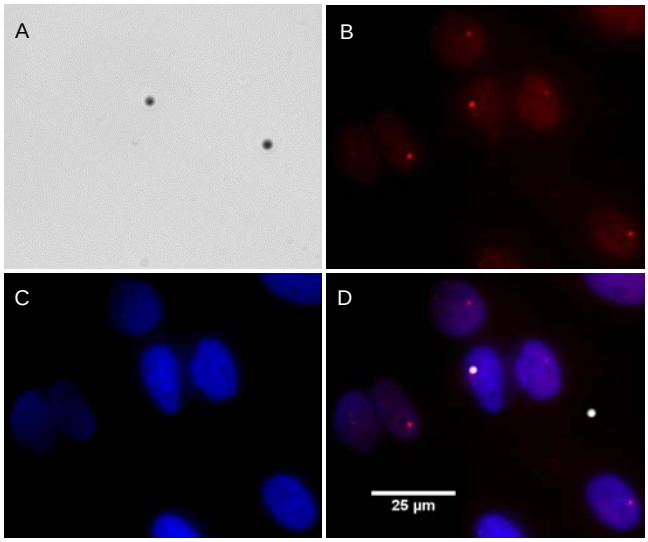
A
B
C
D
25 µm

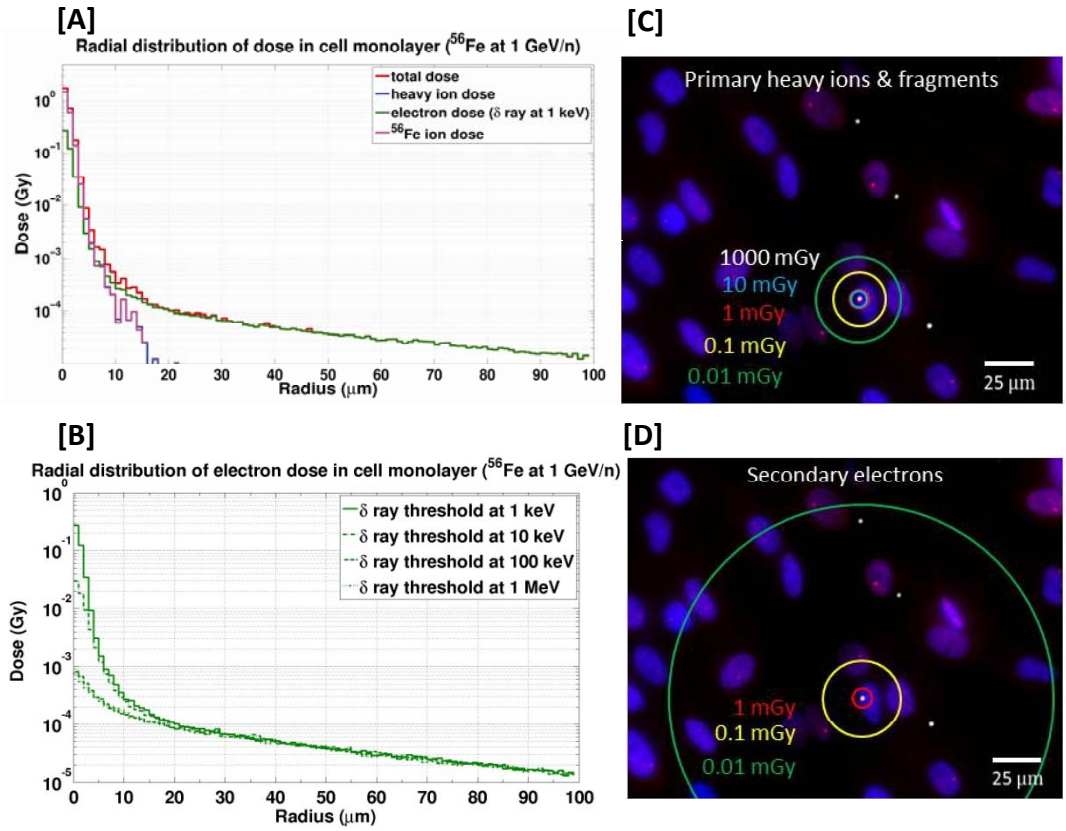
[A]
Radial distribution of dose in cell monolayer (^{56}Fe at 1 GeV/n)
total dose
heavy ion dose
electron dose (δ ray at 1 keV)
^{56}Fe ion dose
Dose (Gy)
Radius (μm)
[B]
Radial distribution of electron dose in cell monolayer (^{56}Fe at 1 GeV/n)
δ ray threshold at 1 keV
δ ray threshold at 10 keV
δ ray threshold at 100 keV
δ ray threshold at 1 MeV
Dose (Gy)
Radius (μm)
[C]
Primary heavy ions & fragments
1000 mGy
10 mGy
1 mGy
0.1 mGy
0.01 mGy
25 μm
[D]
Secondary electrons
1 mGy
0.1 mGy
0.01 mGy
25 μm

[A] Glass-bottomed flaskette

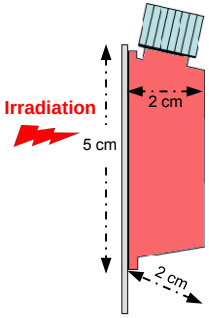

[B] Tissue culture dish with 100 µm-thick PADC plastic grafted

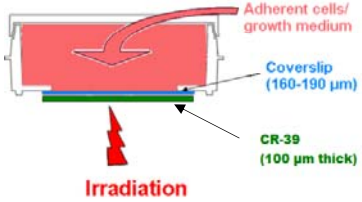

Table 1: Estimates[a] of particle traversals when confluent AG1522 normal human fibroblasts are exposed to mean absorbed dose of 0.2 cGy from radiations that differ in their energy and linear energy transfer (LET)

Ion[b]	Energy (*MeV/u*)	LET (*keV/µm*)	Dose (*cGy*)	Fluence (*particles/cm²*)	**Average number of traversals**		**Fraction of cell nuclei traversed by 0, 1 or more than 1 particles**		
					Cell	**Nucleus**	P(0)	P(1)	P(≥2)
$^{56}Fe^{26+}$	1000	151	0.2	8.27×10^3	0.066	0.012	0.988	0.011	0.001
			1.0	4.13×10^4	0.331	0.058	0.944	0.055	0.001
$^{28}Si^{14+}$	600	50	0.2	2.50×10^4	0.200	0.035	0.966	0.033	0.001
			1.0	1.25×10^5	0.999	0.175	0.840	0.147	0.013
$^{12}C^{6+}$	290	13	0.2	9.60×10^4	0.768	0.134	0.874	0.118	0.008
			1.0	4.80×10^5	3.841	0.672	0.511	0.343	0.146
$^{4}He^{2+}$ (α)	0.92	109	0.2	1.15×10^4	0.092	0.016	0.984	0.016	0.000
			1.0	5.72×10^4	0.458	0.080	0.923	0.074	0.003

[a] These estimates do not take into account secondary radiations.

[b] Note that the primary ions are stripped of electrons. The charge is implied, but not designated, elsewhere in this publication.

Table 2: Contribution of primary and secondary particles to the mean absorbed dose in the *cell monolayer* (0.001 cm^3) when 1000 MeV/u ^{56}Fe, 600 MeV/u ^{28}Si, or 290 MeV/u ^{12}C ions are used to deliver 0.2 cGy to the AG1522 cell culture.

	^{56}Fe		^{28}Si		^{12}C	
Particles[a]	Absorbed Dose[b] (*cGy*)	Contribution to total dose *(%)*	Absorbed Dose[b] (cGy)	Contribution to total dose (%)	Absorbed Dose[b] (cGy)	Contribution to total dose (%)
HZE primary	0.1221	59.87	0.1232	60.96	0.1268	62.06
HZE fragments	0.0007	0.35	0.0004	0.20	0.0002	0.09
Electrons	0.0807	39.57	0.0777	38.44	0.0755	36.94
Photons	2.2013×10^{-6}	0.00	1.1169×10^{-6}	0.00	8.7095×10^{-7}	0.00
Protons	2.3514×10^{-4}	0.12	4.7413×10^{-4}	0.23	1.0729×10^{-3}	0.53
Alpha	5.1070×10^{-5}	0.03	1.4144×10^{-4}	0.07	3.5004×10^{-4}	0.17
Total	**0.2039**	**100.00**	**0.2021**	**100.00**	**0.2043**	**100**

[a] Production thresholds for δ rays were set at 1 keV. Transport cut-offs were set at 150 eV for electrons and 1 keV for HZE particles, protons, photons and α particles.
[b] Errors in the absorbed doses are detailed in Supplementary Tables 2-4.

Supplementary Table 1: Results of Western Blot analyses of p-TP53ser15, p-ERK1/2, $p21^{Waf1}$, HDM2, protein carbonylation and lipid peroxidation related to the data in [A] Figure 1, [B] Figure 2 and [C] Figure 3, after exposure of AG1522 cells to an absorbed dose of 0, 0.2 or 1 cGy from 1000 MeV/u ^{56}Fe ions, 600 MeV/u ^{28}Si ions or 3.7 MeV α particles.

The number of individual experiment, averaged data and associated errors are noted.

[A] In confluent cell cultures

Particles	*Dose*	*Time*	*Protein*	*Fold increase relative to control*	*n*	*Mean*	*Standard Error (SE)*
3.7 MeV α particles	0.2 cGy	15 min	p-TP53ser15	1.5/1.4/1.4/1.5	4	1.5	0.0
	0.2 cGy	15 min	p-ERK1/2	1.3/1.2/1.1	3	1.2	0.1
	0.2 cGy	3 h	$p21^{Waf1}$	1.4/2/1.6	3	1.7	0.2
	1 cGy	15 min	p-TP53ser15	3.3/1.8/2/1.5/2.8/1.7/1.6	7	2.1	0.3
	1 cGy	15 min	p-ERK1/2	1.6/2/2.2/1.8/2.9/2.4	6	2.2	0.2
	1 cGy	3 h	$p21^{Waf1}$	3/1.6/3.6/2.6/2.4/3	6	2.7	0.3
1000 MeV/u ^{56}Fe ions	0.2 cGy	15 min	p-TP53ser15	1.2/1.3/2.5	3	1.7	0.4
	0.2 cGy	15 min	p-ERK1/2	1.6/1.2/1.3	3	1.4	0.1
	0.2 cGy	1 h	HDM2	2.4/1.5/2.2	3	2.0	0.3
	0.2 cGy	1 h	$p21^{Waf1}$	3/3.2/1.5	3	2.6	0.5
	0.2 cGy	1 h	p-TP53ser15	1.6/1.5/1.4	3	1.5	0.1
	0.2 cGy	3 h	$p21^{Waf1}$	2.8/1.7/1.2/1.6/1.3	5	1.7	0.3
	0.2 cGy	6 h	p-TP53ser15	1.8/1.2	2	1.5	0.3
	0.2 cGy	6 h	$p21^{Waf1}$	2.2/1.2/1.7	3	1.7	0.3
	0.2 cGy	24 h	$p21^{Waf1}$	1.6/1.2/1.4	3	1.4	0.1
	0.2 cGy	24 h	p-TP53ser15	1.3/1.4/1.4	3	1.4	0.0
	1 cGy	15 min	p-TP53ser15	1.8/2.4/1.8/7.9/2.8/2.6	6	3.2	1.0
	1 cGy	15 min	p-ERK1/2	2.5/2.9/2.2/4/2.1	5	2.7	0.3
	1 cGy	1 h	HDM2	3.5/2.3/2.2/2.5/2.5/1.4	6	2.4	0.3
	1 cGy	1 h	$p21^{Waf1}$	5.6/1.8/1.6	3	3.0	1.3
	1 cGy	1 h	p-TP53ser15	1.8/1.6/2.6	3	2	0.3
	1 cGy	3 h	$p21^{Waf1}$	3.7/2/2.5/1.7/2.4	5	2.5	0.3
	1 cGy	6 h	p-TP53ser15	2/2.3	2	2.2	0.2
	1 cGy	6 h	$p21^{Waf1}$	3.2/2.4/1.3	3	2.3	0.6
	1 cGy	24 h	$p21^{Waf1}$	6/3.7/5	3	4.9	0.7
	1 cGy	24 h	p-TP53ser15	2.3/5.1/2.2	3	3.2	1.0
600 MeV/u ^{28}Si ions	0.2 cGy	15 min	p-TP53ser15	2.5/3.1/1.3	3	2.3	0.5
	0.2 cGy	15 min	p-ERK1/2	1.4/1.5/1.2	3	1.4	0.1
	0.2 cGy	3 h	$p21^{Waf1}$	1.8/1.2/1.1	3	1.4	0.2
	1 cGy	15 min	p-TP53ser15	3.4/2.4/1.6/4	4	2.9	0.5
	1 cGy	15 min	p-ERK1/2	3.1/2.1/2.8/1.6	4	2.4	0.3
	1 cGy	3 h	$p21^{Waf1}$	2.5/2.3/2.2	3	2.3	0.1

[B] In confluent cell cultures

Particles	*Dose*	*Time*	*Protein*	*Fold increase relative to control*	*n*	*Mean*	*Standard Error (SE)*
1000 MeV/u ^{56}Fe ions	0.2 cGy	24 h	Protein Carbonylation	2.3/6/1.5	3	3.3	1.4
	0.2 cGy	24 h	Lipid peroxydation	1.7/1.4/2.2	3	1.8	0.2
	1 cGy	24 h	Protein Carbonylation	4.1/10/5.5	3	6.5	1.8
	1 cGy	24 h	Lipid peroxydation	6.6/2.1/2.8	3	3.8	1.4

[C] In proliferating cells

Particles	*Dose*	*Time*	*Protein*	*Fold increase relative to control*	*n*	*Mean*	*Standard Error (SE)*
1000 MeV/u ^{56}Fe ions	1 cGy	8 h	p-TP53ser15	1.4/1.2/1.5/1.9	4	1.5	0.1
	1 cGy	8 h	$p21^{Waf1}$	2.4/1.3/1.4/1.8/1.8	5	1.7	0.2
	1 cGy	8 h	HDM2	1.8/1.7/1.6	3	1.7	0.1
	1 cGy	24 h	p-TP53ser15	1.5/1.2/2.3/1.3	4	1.6	0.2
	1 cGy	24 h	$p21^{Waf1}$	1.8/2.1/1.5/1.1	4	1.6	0.2
	1 cGy	24 h	HDM2	1.5/2.5/1.1/2.7/1.3	5	1.8	0.3

Supplementary Table 2: Contribution of primary and secondary particles to the mean absorbed dose in the glass coverslip, cell culture and medium when 1000 MeV/u ^{56}Fe ions were used to deliver 0.2 cGy to the AG1522 cell culture. The production thresholds of δ rays were set at [A] 1 keV, [B] 10 keV, [C] 100 keV, [D] 1 MeV. The transport cut-off was set at 1 keV for HZE particles, protons, photons, and α particles. For electrons, it was set at 150 eV (Panel A) or 1 keV (Panels B, C and D).

[A]

1 keV	**Glass coverslip (1.9152 cm^3)**	**Cell Monolayer (0.001 cm^3)**		**Medium (water) (18.799 cm^3)**
Particles	**Absorbed Dose (*cGy*)**	**Absorbed Dose (*cGy*)**	**Contribution to total dose *%***	**Absorbed Dose (*cGy*)**
Total heavy ions	0.1000 ± 0.0007	0.1228 ± 0.0022	60.22 *0.35*	0.1185 ± 0.0022
^{56}Fe ions	0.0997 ± 0.0007	0.1221 ± 0.0022	59.87	0.1114 ± 0.0022
Electrons	0.0623 ± 0.0004	0.0807 ± 0.0014	39.57	0.0756 ± 0.0014
Photons	3.2609 x 10^{-6} ± 0.69 %	2.2013 x 10^{-6} ± 82.22 %	0.00	2.3844 x 10^{-6} ± 1.11 %
Protons	1.2438 x 10^{-4} ± 8.72 %	2.3514 x 10^{-4} ± 21.97 %	0.12	5.1421 x 10^{-4} ± 2.57 %
Alpha	4.3250 x 10^{-5} ± 16.40 %	5.1070 x 10^{-5} ± 102.92 %	0.03	1.5104 x 10^{-4} ± 3.47 %
Total	**0.1626 ± 0.0012**	**0.2039 ± 0.0036**	**100**	**0.1950 ± 0.0036**

[B]

10 keV	**Glass coverslip (1.9152 cm^3)**	**Cell Monolayer (0.001 cm^3)**		**Medium (water) (18.799 cm^3)**
Particles	**Absorbed Dose (*cGy*)**	**Absorbed Dose (*cGy*)**	**Contribution to total dose *%***	**Absorbed Dose (*cGy*)**
Total heavy ions	0.1206 ± 0.0011	0.1452 ± 0.0020	71.67 *0.44*	0.1404 ± 0.0019
^{56}Fe ions	0.1202 ± 0.0011	0.1443 ± 0.0020	71.23	0.1320 ± 0.0018
Electrons	0.0412 ± 0.0004	0.0569 ± 0.0009	28.08	0.0529 ± 0.0007
Photons	2.7719 x 10^{-6} ± 0.92 %	1.9991 x 10^{-6} ± 14.62 %	0.00	2.1064 x 10^{-6} ± 1.35 %
Protons	1.6855 x 10^{-4} ± 7.96 %	2.8335 x 10^{-4} ± 16.52 %	0.14	6.1175 x 10^{-4} ± 3.49 %
Alpha	5.7126 x 10^{-5} ± 16.36 %	9.6370 x 10^{-5} ± 57.56 %	0.05	1.7112 x 10^{-4} ± 4.38 %
Total	**0.1622 ± 0.0015**	**0.2025 ± 0.0029**	**100**	**0.1943 ± 0.0026**

[C]

100 keV	**Glass coverslip (1.9152 cm^3)**	**Cell Monolayer (0.001 cm^3)**		**Medium (water) (18.799 cm^3)**
Particles	**Absorbed Dose (*cGy*)**	**Absorbed Dose (*cGy*)**	**Contribution to total dose *%***	**Absorbed Dose (*cGy*)**
Total heavy ions	0.1420 ± 0.0008	0.1698 ± 0.0018	84.94 *0.48*	0.1642 ± 0.0018
^{56}Fe ions	0.1416 ± 0.0008	0.1688 ± 0.0018	84.46	0.1546 ± 0.0016
Electrons	0.0198 ± 0.0.001	0.0294 ± 0.0004	14.72	0.0301 ± 0.0003
Photons	1.5099×10^{-6} ± 0.79 %	1.0620×10^{-6} ± 74.71 %	0.00	1.3329×10^{-6} ± 2.33 %
Protons	1.8447×10^{-4} ± 8.36 %	3.5205×10^{-4} ± 12.33 %	0.18	7.0077×10^{-4} ± 2.84 %
Alpha	5.6496×10^{-5} ± 13.10 %	1.5287×10^{-4} ± 98.28 %	0.08	1.9140×10^{-4} ± 4.40 %
Total	**0.1622 ± 0.0009**	**0.1999 ± 0.0021**	**100**	**0.1954 ± 0.0021**

[D]

1 MeV	**Glass coverslip (1.9152 cm^3)**	**Cell Monolayer (0.001 cm^3)**		**Medium (water) (18.799 cm^3)**
Particles	**Absorbed Dose (*cGy*)**	**Absorbed Dose (*cGy*)**	**Contribution to total dose *%***	**Absorbed Dose (*cGy*)**
Total heavy ions	0.1633 ± 0.0008	0.1922 ± 0.0027	97.66 *0.61*	0.1858 ± 0.0016
^{56}Fe ions	0.1628 ± 0.0008	0.1910 ± 0.0028	97.05	0.1751 ± 0.0016
Electrons	0.0016 ± 0.72 %	0.0040 ± 0.0001	2.03	0.0069 ± 0.0001
Photons	3.0758×10^{-7} ± 2.36 %	4.9817×10^{-8} ± 75.16 %	0.00003	1.7904×10^{-7} ± 14.80 %
Protons	2.0372×10^{-4} ± 7.36 %	3.4352×10^{-4} ± 8.05 %	0.17	7.4120×10^{-4} ± 3.54 %
Alpha	6.1595×10^{-5} ± 12.03 %	1.1259×10^{-4} ± 78.06 %	0.05	2.0916×10^{-4} ± 4.68 %
Total	**0.1653 ± 0.0008**	**0.1968 ± 0.0029**	**100**	**0.1939 ± 0.0016**

Errors represent standard deviations of the mean. When the standard deviation is < 0.0001 cGy, it is expressed and noted in % as it can represent a high deviation. The term “total heavy ion” refers to the primary 1000 MeV/u ^{56}Fe ions and the fragments.

Supplementary Table 3: Contribution of primary and secondary particles to the mean absorbed dose in the glass coverslip, cell culture and medium when 600 MeV/u ^{28}Si ions were used to deliver 0.2 cGy to the AG1522 cell culture. The production thresholds of δ rays were set at [A] 1 keV, [B] 10 keV, [C] 100 keV, [D] 1 MeV. The transport cut-off was set at 1 keV for HZE particles, protons, photons, and α particles. For electrons, it was set at 150 eV (Panel A) or 1 keV (Panels B, C and D).

[A]

1 keV	**Glass coverslip (1.9152 cm^3)**	**Cell Monolayer (0.001 cm^3)**		**Medium (water) (18.799 cm^3)**
Particles	**Absorbed Dose (*cGy*)**	**Absorbed Dose (*cGy*)**	**Contribution to total dose *%***	**Absorbed Dose (*cGy*)**
Total heavy ions	0.1006 ± 0.0003	0.1236 ± 0.0012	61.16 *0.20*	0.1209 ± 0.0004
^{28}Si ions	0.1003 ± 0.0010	0.1232 ± 0.0012	60.96	0.1170 ± 0.0012
Electrons	0.0611 ± 0.0006	0.0777 ± 0.0012	38.44	0.0720 ± 0.0007
Photons	3.1033 x 10^{-6} ± 1.40 %	1.1169 x 10^{-6} ± 82.11 %	0.00	2.1527 x 10^{-6} ± 2.25 %
Protons	2.7759 x 10^{-4} ± 5.06 %	4.7413 x 10^{-4} ± 26.76 %	0.23	9.7519 x 10^{-4} ± 5.20 %
Alpha	1.0644 x 10^{-4} ± 13.94 %	1.4144 x 10^{-4} ± 73.98 %	0.07	2.6864 x 10^{-4} ± 5.03 %
Total	**0.1622 ± 0.0016**	**0.2021 ± 0.0024**	**100**	**0.1945 ± 0.0019**

[B]

10 keV	**Glass coverslip (1.9152 cm^3)**	**Cell Monolayer (0.001 cm^3)**		**Medium (water) (18.799 cm^3)**
Particles	**Absorbed Dose (*cGy*)**	**Absorbed Dose (*cGy*)**	**Contribution to total dose *%***	**Absorbed Dose (*cGy*)**
Total heavy ions	0.1218 ± 0.0008	0.1467 ± 0.0014	73.11 *0.26*	0.1436 ± 0.0016
^{28}Si ions	0.1215 ± 0.0008	0.1462 ± 0.0014	72.85	0.1389 ± 0.0016
Electrons	0.0392 ± 0.0003	0.0531 ± 0.0009	26.44	0.0479 ± 0.0005
Photons	2.5971 x 10^{-6} ± 0.75 %	1.0276 x 10^{-6} ± 54.41 %	0.00	1.8470 x 10^{-6} ± 2.18 %
Protons	3.4229 x 10^{-4} ± 7.30 %	5.7103 x 10^{-4} ± 22.19 %	0.28	1.2144 x 10^{-3} ± 3.40 %
Alpha	1.2456 x 10^{-4} ± 8.93 %	1.0788 x 10^{-4} ± 82.28 %	0.05	3.4464 x 10^{-4} ± 4.14 %
Total	**0.1617 ± 0.0010**	**0.2007 ± 0.0023**	**100**	**0.1934 ± 0.0021**

[C]

100 keV	**Glass coverslip (1.9152 cm^3)**	**Cell Monolayer (0.001 cm^3)**		**Medium (water) (18.799 cm^3)**
Particles	**Absorbed Dose (*cGy*)**	**Absorbed Dose (*cGy*)**	**Contribution to total dose *%***	**Absorbed Dose (*cGy*)**
Total heavy ions	0.1434 ± 0.0004	0.1708 ± 0.0011	86.74 *0.31*	0.1671 ± 0.0014
^{28}Si ions	0.1431 ± 0.0012	0.1702 ± 0.0011	86.43	0.1616 ± 0.0013
Electrons	0.0175 ± 0.0.001	0.0250 ± 0.0003	12.70	0.0241 ± 0.0002
Photons	1.3178×10^{-6} ± 0.90 %	6.7873×10^{-7} ± 157.79 %	0.00	1.0610×10^{-6} ± 2.89 %
Protons	3.9845×10^{-4} ± 7.79 %	7.0894×10^{-4} ± 14.22 %	0.36	1.3842×10^{-3} ± 1.63 %
Alpha	1.3043×10^{-4} ± 12.69 %	1.8740×10^{-4} ± 67.54 %	0.10	3.4464×10^{-4} ± 4.14 %
Total	**0.1616 ± 0.0014**	**0.1969 ± 0.0013**	**100**	**0.1933 ± 0.0016**

[D]

1 MeV	**Glass coverslip (1.9152 cm^3)**	**Cell Monolayer (0.001 cm^3)**		**Medium (water) (18.799 cm^3)**
Particles	**Absorbed Dose (*cGy*)**	**Absorbed Dose (*cGy*)**	**Contribution to total dose *%***	**Absorbed Dose (*cGy*)**
Total heavy ions	0.1633 ± 0.0012	0.1938 ± 0.0041	98.43 *0.36*	0.1887 ± 0.0030
^{28}Si ions	0.1630 ± 0.0122	0.1931 ± 0.0409	98.07	0.1827 ± 0.0296
Electrons	0.0007 ± 0.0000	0.0019 ± 0.0001	0.96	0.0027 ± 0.0000
Photons	1.4358×10^{-7} ± 5.34 %	1.8106×10^{-8} ± 210.82 %	0.00	6.5495×10^{-8} ± 20.30 %
Protons	3.7917×10^{-4} ± 9.00 %	6.5103×10^{-4} ± 14.40 %	0.48	1.4250×10^{-3} ± 3.29 %
Alpha	1.3149×10^{-4} ± 11.76 %	1.1953×10^{-4} ± 38.38 %	0.06	3.8005×10^{-4} ± 4.26 %
Total	**0.1647 ± 0.0012**	**0.1969 ± 0.0041**	**100**	**0.1937 ± 0.0031**

Errors represent standard deviations of the mean. When the standard deviation is <0.0001 cGy, it is expressed and noted in % as it can represent a high deviation. The term “total heavy ion” refers to the primary 600 MeV/u ^{28}Si ions and the fragments.

Supplementary Table 4: Contribution of primary and secondary particles to the mean absorbed dose in the glass coverslip, cell culture and medium when 290 MeV/u ^{12}C ions are used to deliver 0.2 cGy to the AG1522 cell culture. The production thresholds of δ rays were set at [A] 1 keV, [B] 10 keV, [C] 100 keV, [D] 1 MeV. The transport cut-off was set at 1 keV for HZE particles, protons, photons and α particles. For electrons, it was set at 150 eV (Panel A) or 1 keV (Panels B, C and D).

[A]

1 keV	**Glass coverslip (1.9152 cm^3)**	**Cell Monolayer (0.001 cm^3)**		**Medium (water) (18.799 cm^3)**
Particles	**Absorbed Dose (*cGy*)**	**Absorbed Dose (*cGy*)**	**Contribution to total dose *%***	**Absorbed Dose (*cGy*)**
Total heavy ions	0.1024 ± 0.0001	0.1270 ± 0.0013	62.15 *0.09*	0.1265 ± 0.0001
^{12}C ions	0.1023 ± 0.0006	0.1268 ± 0.0013	62.06	0.1249 ± 0.0011
Electrons	0.0613 ± 0.0004	0.0755 ± 0.0015	36.94	0.0710 ± 0.0006
Photons	3.0082 x 10^{-6} ± 0.93 %	8.7095 x 10^{-7} ± 138.13 %	0.00	1.9454 x 10^{-6} ± 2.67 %
Protons	6.0239 x 10^{-4} ± 10.79 %	1.0729 x 10^{-3} ± 34.90 %	0.53	2.2658 x 10^{-3} ± 4.59 %
Alpha	2.6778 x 10^{-4} ± 15.20 %	3.5004 x 10^{-4} ± 84.32 %	0.17	7.1590 x 10^{-4} ± 4.49 %
Total	**0.1649 ± 0.0011**	**0.2043 ± 0.0029**	**100**	**0.2011 ± 0.0018**

[B]

10 keV	**Glass coverslip (1.9152 cm^3)**	**Cell Monolayer (0.001 cm^3)**		**Medium (water) (18.799 cm^3)**
Particles	**Absorbed Dose (*cGy*)**	**Absorbed Dose (*cGy*)**	**Contribution to total dose *%***	**Absorbed Dose (*cGy*)**
Total heavy ions	0.1256 ± 0.0010	0.1525 ± 0.0019	74.89 *0.21*	0.1521 ± 0.0019
^{12}C ions	0.1254 ± 0.0010	0.1521 ± 0.0020	74.68	0.1501 ± 0.0019
Electrons	0.0378 ± 0.0003	0.0490 ± 0.0009	24.05	0.0443 ± 0.0005
Photons	2.4343 x 10^{-6} ± 1.24 %	9.3402 x 10^{-7} ± 105.77 %	0.00	1.6359 x 10^{-6} ± 4.67 %
Protons	7.7265 x 10^{-4} ± 14.18 %	1.3566 x 10^{-3} ± 36.62 %	0.67	2.7321 x 10^{-3} ± 4.26%
Alpha	3.5199 x 10^{-4} ± 13.32 %	2.3531 x 10^{-4} ± 98.87 %	0.12	7.0770 x 10^{-4} ± 5.66 %
Total	**0.1648 ± 0.0013**	**0.2037 ± 0.0030**	**100**	**0.2007 ± 0.0024**

[C]

100 keV	**Glass coverslip (1.9152 cm^3)**	**Cell Monolayer (0.001 cm^3)**		**Medium (water) (18.799 cm^3)**
Particles	**Absorbed Dose (*cGy*)**	**Absorbed Dose (*cGy*)**	**Contribution to total dose *%***	**Absorbed Dose (*cGy*)**
Total heavy ions	0.1489 ± 0.0001	0.1787 ± 0.0033	88.92 *0.20*	0.1772 ± 0.0015
^{12}C ions	0.1486 ± 0.0012	0.1783 ± 0.0032	88.72	0.1749 ± 0.0016
Electrons	0.0148 ± 0.001	0.0198 ± 0.0006	9.86	0.0183 ± 0.0002
Photons	1.1053×10^{-6} ± 1.82 %	3.7904×10^{-7} ± 170.03 %	0.00	7.8355×10^{-7} ± 5.69 %
Protons	8.5832×10^{-4} ± 14.21 %	1.5021×10^{-3} ± 21.36 %	0.75	3.0876×10^{-3} ± 4.44 %
Alpha	3.4244×10^{-4} ± 15.08 %	4.6763×10^{-4} ± 59.71 %	0.23	9.3214×10^{-4} ± 6.61 %
Total	**0.1653 ± 0.0013**	**0.2009 ± 0.0031**	**100**	**0.2004 ± 0.0018**

[D]

1 MeV	**Glass coverslip (1.9152 cm^3)**	**Cell Monolayer (0.001 cm^3)**		**Medium (water) (18.799 cm^3)**
Particles	**Absorbed Dose (*cGy*)**	**Absorbed Dose (*cGy*)**	**Contribution to total dose *%***	**Absorbed Dose (*cGy*)**
Total heavy ions	0.1654 ± 0.0013	0.1971 ± 0.0038	98.30 *0.15*	0.1958 ± 0.0014
^{12}C ions	0.1652 ± 0.0014	0.1910 ± 0.0038	98.15	0.1934 ± 0.0013
Electrons	5.0037×10^{-7} ± 73.15 %	7.0334×10^{-7} ± 83.07 %	0.00	1.7944×10^{-6} ± 26.38 %
Photons	3.2179×10^{-7} ± 101.49 %	0.0000 ± 0.0000	0.00	1.6590×10^{-11} ± 78.71 %
Protons	7.5727×10^{-5} ± 11.64 %	1.5147×10^{-4} ± 26.84 %	0.08	2.8089×10^{-4} ± 3.62 %
Alpha	3.4659×10^{-4} ± 16.25 %	6.5669×10^{-4} ± 0.0006	0.33	9.9823×10^{-4} ± 7.15 %
Total	**0.1670 ± 0.0014**	**0.2005 ± 0.0037**	**100**	**0.2010 ± 0.0013**

Errors represent standard deviations of the mean. When the standard deviation is <0.0001 cGy, it is expressed and noted in % as it can represent a high deviation. The term “total heavy ion” refers to the primary 290 MeV/u ^{12}C ions and the fragments.